J BONE ONCOL 50 (2025) 100655

Contents lists available at ScienceDirect

Journal of Bone Oncology

journal homepage: www.elsevier.com/locate/jbo

Research Paper

Using β-Elemene to reduce stemness and drug resistance in osteosarcoma: A focus on the AKT/FOXO1 signaling pathway and immune modulation

Shaochun Zhang [a,1,*], Zhijie Xing [a,1], Jing Ke [b]

[a] Orthopedics Department, The Central Hospital of Ezhou, Ezhou 436000, China
[b] Department of Endocrinology, The Central Hospital of Ezhou, Ezhou 436000, China

HIGHLIGHTS

- First report: β-elemene activates M1 macrophage inflammation via AKTFOXO1 in osteosarcoma.
- β-elemene targets osteosarcoma stem cells,suppressing their stemness.
- β-elemene enhances osteosarcoma sensitivity to DOX chemotherapy.
- AKT1 identified as osteosarcoma progression key gene by bioinformatics.
- New targets and strategies for osteosarcoma treatment uncovered.

ARTICLE INFO

Keywords:
β-Elemene
Osteosarcoma
Drug Resistance
Protein Kinase B/Forkhead Box O1 Signaling Pathway
M1 Type Macrophages

ABSTRACT

Objective: Osteosarcoma, a highly malignant bone tumor, poses significant treatment challenges due to its propensity for stemness and drug resistance, particularly against doxorubicin (DOX). This study aims to investigate the mechanism by which β-elemene reduces the stemness of osteosarcoma stem cells and ultimately decreases DOX resistance by inhibiting the Akt/FoxO1 signaling pathway and activating a macrophage-mediated inflammatory microenvironment.

Methods: Osteosarcoma stem cells were isolated and induced for DOX resistance. *In vitro* and *in vivo* models were employed to assess β-elemene's impact on cell viability, stemness, and drug resistance. Bioinformatics analysis, flow cytometry, and immunofluorescence staining were used to evaluate signaling pathway activity and macrophage polarization. Additionally, an osteosarcoma xenograft mouse model was established to confirm the therapeutic effects of β-elemene.

Results: In vivo animal experiments demonstrated that β-elemene reduces osteosarcoma resistance. Bioinformatics analysis revealed that AKT1 is a key core gene in osteosarcoma progression, acting through the FOXO signaling pathway. Additionally, AKT inhibits immune cell infiltration in osteosarcoma and suppresses immune responses during osteosarcoma progression. β-elemene may influence osteosarcoma progression by mediating TP53 to regulate PTEN and subsequently AKT1. *In vitro* experiments showed that β-elemene promotes M1 macrophage activation by inhibiting the Akt/FoxO1 signaling axis, thereby reducing the stemness of osteosarcoma stem cells. Finally, *in vivo* animal experiments confirmed that β-elemene reduces osteosarcoma resistance by promoting M1 macrophage activation through inhibition of the Akt/FoxO1 signaling axis.

Conclusion: β-Elemene demonstrates promising potential in reducing osteosarcoma stemness and drug resistance via dual mechanisms: targeting the AKT/FOXO1 pathway and modulating the tumor immune microenvironment. These findings suggest β-elemene as a potential adjunct therapy for osteosarcoma, providing novel therapeutic strategies to overcome chemotherapy resistance and improve patient outcomes.

Abbreviations: AKT, Protein Kinase B; ANOVA, Analysis of Variance; BP, Biological Process; cDNA, Complementary DNA; CC, Cellular Component; DEGs, Differentially Expressed Genes; DOX, Doxorubicin; FOXO1, Forkhead Box O1; GO, Gene Ontology; KEGG, Kyoto Encyclopedia of Genes and Genomes; MAD, Median Absolute Deviation; MF, Molecular Function; OD, Optical Density; PBS, Phosphate-Buffered Saline; PFA, Paraformaldehyde; PPI, Protein-Protein Interaction; RT-qPCR, Real-Time Quantitative PCR; SD, Standard Deviation; WB, Western Blot; WGCNA, Weighted Gene Co-expression Network Analysis; 5-FU, 5-Fluorouracil.

* Corresponding author at: Orthopedics Department, The Central Hospital of Ezhou, No.9 Wenxing Road, Echeng District, Ezhou 436000, Hubei Province, China.
E-mail address: sczhangdoctor@126.com (S. Zhang).

[1] These authors are regarded as co-first authors.

https://doi.org/10.1016/j.jbo.2024.100655
Received 26 September 2024; Received in revised form 2 December 2024; Accepted 10 December 2024
Available online 19 December 2024

1. Introduction

Osteosarcoma is a highly malignant bone tumor primarily affecting adolescents and children, characterized by rapid growth and aggressive invasion [1,2]. Although modern comprehensive treatment methods have improved long-term survival rates, the prognosis remains poor for patients with recurrent or metastatic osteosarcoma [3,4]. Currently, the main therapeutic approaches for osteosarcoma include surgical resection, radiation therapy, and chemotherapy, with chemotherapy being a critical component [5–7]. However, the effectiveness of chemotherapy is often significantly reduced due to the tumor's resistance to drugs, particularly severe in the case of first-line anticancer drugs like doxorubicin (DOX) [8,9]. Thus, developing new treatment strategies to reduce the pro-tumor properties of drug-resistant cells and enhance therapeutic efficacy is critical in osteosarcoma research [10,11].

Drug resistance in osteosarcoma involves multiple factors and mechanisms [12,13]. Current research indicates that osteosarcoma cells can evade the cytotoxic effects of drugs through various mechanisms, including enhanced activity of drug efflux pumps, alteration of drug targets, repair of drug-induced DNA damage, and the protective role of the tumor microenvironment [14–16]. Additionally, cancer stem cells play a pivotal role in the development of drug resistance due to their self-renewal capabilities, surviving chemotherapy and potentially causing disease relapse or metastasis [17]. Therefore, addressing drug resistance, particularly targeting cancer stem cells and modulating the tumor microenvironment, is key to improving treatment success rates for osteosarcoma [18].

In recent years, β-elemene, a naturally occurring monoterpenoid, has shown broad potential in cancer therapy [19]. Studies have demonstrated β-elemene's capability to inhibit tumor proliferation, induce cancer cell apoptosis, and modulate immune responses across various cancer models [20,21]. Its mechanisms likely involve multiple signaling pathways and molecular targets, such as inducing cell cycle arrest, activating intrinsic apoptotic pathways, and regulating immune cell functions [22,23]. These findings provide a theoretical basis for the application of β-elemene in the treatment of osteosarcoma.

Recently, the role of the tumor microenvironment, particularly the immune microenvironment, has gained increasing attention in cancer therapy [24–26]. Studies have demonstrated that M1 type macrophages play a crucial role in suppressing tumors; they can directly kill tumor cells by secreting pro-inflammatory cytokines or activate other immune cells to participate in anti-tumor responses [27–29]. The Protein Kinase B (AKT)/Forkhead Box O1 (FOXO1) signaling pathway is one of the key routes regulating macrophage polarization, and modulating this pathway can significantly affect macrophage function and thereby the survival environment of tumor cells [30,31]. Thus, investigating this pathway in osteosarcoma offers new therapeutic targets and is of significant clinical importance [32–34].

This study aims to explore how β-elemene activates an M1 macrophage-mediated inflammatory microenvironment through the AKT/FOXO1 signaling pathway and assess its impact on osteosarcoma stem cells' stemness and drug resistance. By understanding the specific mechanisms of β-elemene in regulating macrophage function and exploring its role in blocking the development of drug resistance in osteosarcoma, this research seeks to provide new insights and strategies for treating osteosarcoma. We anticipate that the findings will deepen the understanding of the mechanisms behind osteosarcoma drug resistance and offer theoretical bases and potential targets for drug development, particularly in improving patient outcomes and quality of life.

2. Materials and methods

2.1. Osteosarcoma transcriptome analysis and differential gene expression

The GEO database (https://www.ncbi.nlm.nih.gov/geo/) downloaded transcriptome datasets related to osteosarcoma, specifically dataset GSE99671. This included samples from 18 cases of osteosarcoma and corresponding normal tissues. Normal tissues served as controls, while osteosarcoma samples formed the experimental group. Analysis of differentially expressed genes (DEGs) was conducted using the R package "limma." Genes were selected based on a threshold of $|\log2(\text{FoldChange})| > 0.35$ and a significance p-value < 0.05.

2.2. Disease and drug target identification

Osteosarcoma-related targets were searched in the GeneCards database (https://www.genecards.org/) and the Disgenet database (https://www.disgenet.org/) using the keyword "Osteosarcoma." Retrieved targets were consolidated, removing duplicates to create a set of disease-related targets. Using the TCMSP (https://old.tcmsp-e.com/tcmsp.php), target information for β-elemene was collected. Targets were annotated using the Uniprot website, and duplicates and non-human genes were removed. Additionally, the canonical SMILES for β-elemene (CC(=C)C1CCC(C(C1)C(=C)C)(C)C = C) was retrieved from the PubChem Compound database. Target predictions were performed using the SWISS database (https://www.swisstargetprediction.ch/) to identify the potential targets of β-elemene. Venn diagrams to illustrate the intersections of targets were generated using Xiantao academic online bioinformatics tools.

2.3. Weighted gene co-expression network analysis (WGCNA)

Gene expression profiles were analyzed for median absolute deviation (MAD), excluding the lowest 50 % of genes based on MAD values. Subsequent analysis using the R package "WGCNA" and the goodSamplesGenes function helped remove outlier genes and samples. A scale-free gene co-expression network set the minimum size for gene dendrograms at 50 and sensitivity at 8. Modules closer than a distance of 0.6 were merged, resulting in three co-expression modules. Pearson correlation tests ($p < 0.05$) were used to assess the relationships between these modules and groups, identifying those significantly associated with osteosarcoma for further analysis.

2.4. Immunocyte correlation analysis

Immunocyte infiltration analysis was conducted on transcriptome data using the SangerBox bioinformatics platform, employing the CIBERSORT algorithm to quantify the presence of immune cells in each sample. The correlations among different immune cells were assessed using the Spearman correlation coefficient based on immunocyte score data. The relationships were visualized through heat maps, highlighting the strength and statistical significance of the correlations between various immune cells.

2.5. Protein-protein interaction (PPI) networks construction

The STRING database (https://www.string-db.org/), which compiles experimental data, text-mined results from PubMed abstracts, and predictions from other databases through bioinformatics methods, was used to study protein interactions. Using the STRING database, we conducted PPI analysis on genes within the MEblue module (with a confidence level set at 0.9) and 28 potential target proteins implicated in β-elemene's treatment of osteosarcoma (with a confidence level set at 0.4). The connectivity of each protein was quantified and visualized using R software; a higher number of connections indicates a greater centrality within the network. This analysis helps identify key proteins that play central roles in the mechanisms through which β-elemene may exert its therapeutic effects on osteosarcoma. Interactions between TP53 and AKT1 were analyzed using the Genemania website.

2.6. Drug-target-disease network construction

Using R, we paired the target genes associated with β-elemene with those linked to osteosarcoma to identify their key overlapping targets. To further investigate the mechanisms by which β-elemene treats osteosarcoma, we constructed a "Drug-Target-Disease" network using Cytoscape (version 3.7.2).

2.7. Gene ontology (GO) and kyoto encyclopedia of genes and genomes (KEGG) enrichment analysis

The online analysis website employs the "ClusterProfiler" package in R to conduct GO and KEGG enrichment analyses on candidate target genes or disease-related DEGs, using a significance threshold of $p < 0.05$ for enriched selection. GO analysis includes assessments of biological process (BP), molecular function (MF), and cellular component (CC). This ultimately identifies the primary cellular functions and signaling pathways impacted by candidate target genes and the enrichment pathways associated with disease-related DEGs. Based on the *p*-values, KEGG enrichment analysis of the candidate target genes is performed using the "ClusterProfiler" package in R, with the results depicted in a bubble chart.

2.8. Cell culture and grouping

Osteosarcoma cells (143B, CBP60234) and human monocytes (THP-1, CBP60518) were acquired from Nanjing Cobioer Biosciences Co., Ltd. The cells were cultured in RPMI-1640 medium (11875093, Gibco) supplemented with 10 % fetal bovine serum (12483020, Gibco) and 1 % penicillin–streptomycin (15140148, Gibco) at 37 °C in a 5 % CO_2 environment. THP-1 cells were treated with 10 ng/ml phorbol myristate acetate (PMA) (16561–29-8, Sigma-Aldrich) for 48 h to induce differentiation into macrophages.

Selection of osteosarcoma stem cells: osteosarcoma cells were harvested, washed three times with phosphate-buffered saline (PBS), and then incubated with anti-CD44-FITC (ab30405, Abcam) and anti-CD133-Alexa Fluor® 647 (ab252127, Abcam) at room temperature for 40 min. After another PBS wash, cells were resuspended and sorted using a flow cytometer (BD, USA) to isolate $CD44^+$ $CD133^+$ cells. These cells were used to develop DOX-resistant osteosarcoma stem cells by gradually increasing the concentration of DOX (D1515, Sigma-Aldrich, USA) from 0 to 100 ng/mL, ultimately maintaining them in 24 ng/mL of DOX.

2.9. Cell treatment and grouping

Lentiviral Transduction: Lentivirus-mediated silencing of FOXO1 and its controls (sh-NC, sh-FOXO1-1, sh-FOXO1-2) was constructed. Plasmids (sh-NC: 5′-GACTTCATAAGGCGCATGC-3′, sh-FOXO1-1: 5′-CCGGCAGGACAATAAGTCGAGTTATCTCGAGA-TAACTCGACTTATTGTCCTGTTTTTG-3′, sh-FOXO1-2: 5′-CCGGGCTTA-GACTGTGACATGGAATCTCGAGATTCCATGTCA-CAGTCTAAGCTTTTTG-3′) were provided along with lentiviral packaging services by Sangon Biotech (Shanghai, China). Briefly, plasmids encoding the target gene sequences were co-transfected with helper plasmids into 293 T cells (CRL-3216, ATCC, USA). The viruses were subsequently harvested, amplified, and purified following verification. Cells were seeded at a density of 5×10^5 cells/well for macrophage transduction via lentivirus in 6-well plates. At 50–70 % confluence, cells were transduced with lentivirus (MOI = 10, titer approximately 5×10^6 TU/mL) in RPMI-1640 medium supplemented with polybrene (5 μg/mL) (TR-1003, Merck, USA). Four hours post-transduction, an equal medium volume was added to dilute the polybrene, and the medium was refreshed after 24 h. Transduction efficiency was assessed by the fluorescence reporter gene 48 h post-transduction. Stable transductants were selected using puromycin (5 μg/mL) (A1113803, Thermo Fisher, USA).

Cell Grouping: The groups were as follows: Control (untreated macrophages), β-elemene (macrophages treated with β-elemene), β-elemene + sh-NC (macrophages stably transduced with sh-NC and treated with β-elemene), and β-elemene + sh-FOXO1 (macrophages stably transduced with sh-FOXO1 and treated with β-elemene). β-elemene (A10065, Shanghai Yuanye Bio-Technology Co., Ltd.) was used at a concentration of 200 μM for 48 h.

Co-culture: The various groups of macrophages were co-cultured with osteosarcoma stem cells in a 1:1 ratio in Transwell plates for 48 h to establish a co-culture system that simulates the osteosarcoma microenvironment.

2.10. qRT-PCR

Total RNA was extracted from cells using the Trizol reagent. Complementary DNA (cDNA) was synthesized using the Reverse Transcription Kit (RR047A, Takara, Japan). The SYBR® Premix Ex TaqTM II kit (DRR081, Takara, Japan) was used to set up the reaction system for real-time quantitative PCR (RT-qPCR) conducted on the ABI7500 system (Thermo Fisher, USA). The PCR program was configured as follows: initial denaturation at 95 °C for 30 s, followed by 40 cycles of denaturation at 95 °C for 5 s and annealing at 60 °C for 30 s, with a final extension at 95 °C for 15 s and 60 °C for 60 s, then another extension at 90 °C for 15 s before plotting the amplification curves. GAPDH served as the internal control, with each qRT-PCR reaction set up in triplicate, and the experiment was repeated three times. Gene expression fold changes between experimental and control groups were calculated using the $2^{-\Delta\Delta Ct}$ method: ΔΔCT = ΔCt (experimental group) − ΔCt (control group), where ΔCt = Ct (target gene) − Ct (internal control gene). Ct represents the cycle number at which the fluorescence reaches a preset threshold, indicating logarithmic amplification. Primers used are listed in Table 1.

2.11. Western blot (WB)

Total proteins from tissues and cells were lysed using RIPA lysis buffer containing PMSF (P0013B, Beyotime, Shanghai). Protein concentrations were determined using the BCA Protein Assay Kit (P0010, Beyotime, Shanghai), adjusted to 1 μg/μL, denatured by boiling for 5 min, and stored at −80 °C. Proteins were separated on 8 %-12 % SDS gels via SDS-PAGE and transferred onto PVDF membranes. The membranes were blocked in 5 % non-fat milk at room temperature for at least one hour. Incorporate the appropriate primary antibody and incubate overnight with gentle shaking at 4 °C, including p-AKT (1:1000, ab38449, Abcam), AKT (1:1000, ab8805, Abcam), p-FOXO1 (1:1000, ab259337), FOXO1 (1:1000, ab39670, Abcam), iNOS (1:1000, ab178945, Abcam), CD86 (1:1000, ab239075, Abcam), Arg1 (1:1000, ab133543, Abcam), CD206 (1:1000, ab64693, Abcam), Oct4 (1:1000, ab200834), Sox2 (1:1000, ab92494, Abcam), Nanog (1:1000, ab203919), and β-actin (1:1000, ab8226, Abcam). After retrieving the primary antibody, store it at 4 °C. Wash the membrane three times with 1 × TBST at room temperature, each time for 5 min. Add the HRP-conjugated secondary antibody and incubate with gentle shaking at room temperature for one hour. After retrieving the secondary antibody, store it at 4 °C. The secondary antibodies include Goat anti-rabbit IgG (ab6721, 1:5000, Abcam, UK) or Goat anti-mouse IgG (ab205719, 1:5000, Abcam, UK). Wash the membrane three times with 1 × TBST

Table 1
RT-qPCR primer sequences.

Gene Name	Primer Sequences
FoxO1 (human)	Forward: 5′- GCAGCCGCCACATTCAAC-3′ Reverse: 5′- CAGAACTTAACTTCGCGGGG −3′
GAPDH (human)	Forward: 5′-AATGGGCAGCCGTTAGGAAA-3′ Reverse: 5′- GCGCCCAATACGACCAAATC −3′

buffer at room temperature, each time for 5 min. Apply the ECL reaction fluid (1705062, Bio-Rad, USA) thoroughly over the membrane and let it sit at room temperature for 10 s. Remove excess fluid and place the membrane in the Image Quant LAS 4000C gel imaging system (GE, USA) for band exposure and imaging. Measure the relative intensities of the bands using Image J software, with β-actin as the loading control. Repeat all experiments at least three times.

2.12. ELISA detection

Macrophage supernatants were collected, and mouse tumor tissues were homogenized in 5–10 ml of pre-chilled PBS. The homogenates were further processed using ultrasonication and then centrifuged at 850 × g for 15 min at 4 °C to collect the supernatant for subsequent experiments. Cells were first digested with trypsin, collected by centrifugation, and lysed via ultrasonication; the cell lysates were then centrifuged at 1500 × g for 10 min at 4 °C, and the supernatants were reserved. According to the manufacturer's protocols of the Human TNF-α ELISA Kit (ab181421, Abcam, UK), Human IL-6 ELISA Kit (ab178013, Abcam, UK), and Human IL-10 ELISA Kit (ab185986, Abcam, UK), monoclonal antibodies targeting IL-6, TNF-α, and IL-10 were coated onto a 96-well plate, incubated overnight at 4 °C, blocked for 1 h at room temperature, and washed with PBS. Subsequent steps were performed according to the kit instructions. Optical density (OD) at 450 nm was measured using a spectrophotometer (A51119500C, Thermo Fisher, USA).

2.13. CCK-8

Well-growing cells were seeded at a density of 8×10^3 cells per well in a 96-well plate and incubated in a humidified incubator. At specific time points (24 h, 48 h, and 72 h), 10 μL of CCK-8 solution (96992, Sigma-Aldrich, USA) was added to each well. After incubating for 1 h at 37 °C, the absorbance of each sample was measured at 450 nm using an Epoch microplate spectrophotometer (Bio-Tek, Winooski, VT, USA). Each condition was tested in six replicates, and the experiment was repeated three times.

2.14. Spheroid formation assay

SW480 cells were seeded in Nunclon™ Sphera™ dishes (174945, Thermo Fisher, USA) at a density of 2×10^5 cells per dish in serum-free DMEM containing epidermal growth factor (EGF, PHG0311, Gibco, USA) at 20 ng/mL, basic fibroblast growth factor (P5453, Beyotime, China), and 2 % B27 supplement (C0350, Beyotime, China). The medium was replaced halfway every 7 days, and after 14 days, the number of tumor spheroids was counted under a microscope (Olympus, Japan).

2.15. Transwell assay

Twenty-four hours after different treatments, a Transwell invasion assay was performed. The Transwell inserts were coated with 50 μL of Matrigel (354234, BD Biosciences, USA) and allowed to solidify at 37 °C for 30 min. After coating, the inserts were rinsed with serum-free medium, and cells were resuspended in serum-free medium at a concentration of 2.5×10^4 cells/mL. Each upper chamber received 100 μL of the cell suspension, while the lower chamber was filled with 500 μL of medium supplemented with 10 % FBS. After 24 h, the inserts were removed, and cells in the upper chamber were wiped off with a cotton swab. The remaining cells were fixed with 4 % paraformaldehyde (PFA) at room temperature for 30 min and stained with 0.1 % crystal violet for 30 min. Cells were photographed under an inverted microscope (IXplore Pro, Olympus, Japan) in five random fields to count the number of cells. The experiment was repeated three times. The cell migration assay followed the same steps but without the addition of Matrigel.

2.16. Flow cytometry

Apoptosis Detection: Tumor cells (1×10^5/well) were collected and washed with cold PBS, then stained in the dark for 15 min using an apoptosis detection kit (APOAF-20TST, Sigma-Aldrich, USA). Cells were resuspended in 400 μL of binding buffer and stained with 5 μL of Annexin-V from the kit. Flow cytometry was used to analyze the cells. Cells in the upper right quadrant (Annexin V + PI +) represent late apoptotic cells; lower right quadrant (Annexin V + PI-) early apoptotic cells; upper left quadrant (Annexin V-PI +) necrotic cells; and lower left quadrant (Annexin V-PI-) viable cells.

Cell Cycle Analysis: Cells from each group were collected and resuspended in PBS. The cell cycle was analyzed using a cell cycle detection kit (C1052, Beyotime). Samples were treated with RNase A (10 mg/mL) and PI (5 mg/mL) in the dark and incubated at room temperature for 30 min. Samples were then transferred to 5 mL flow cytometry tubes and analyzed using a flow cytometer. DNA content analysis was performed using FlowJo software.

2.17. In vivo tumorigenesis experiment

Twenty-four male NOD/SCID mice (4–6 weeks old, 15–25 g) were procured from Beijing Vital River Laboratory Animal Technology Co., Ltd. (Beijing, China) and housed in cages within an SPF-level animal laboratory. The NOD-SCID mice were acclimatized for one week and monitored for health status. The experimental protocol and animal use were approved by the Institutional Animal Care and Use Committee of our hospital (Ethical Approval Number: L2022-K-05).

DOX-resistant osteosarcoma stem cells (1×10^6 cells) were suspended in 100 μL of PBS and subcutaneously injected into the right axilla of mice. The mice were randomly divided into four groups: the Control group (injected with DOX-resistant osteosarcoma stem cells and gavaged with normal saline), the β-elemene group (injected with DOX-resistant osteosarcoma stem cells and gavaged with β-elemene), the β-elemene + sh-NC group (injected with DOX-resistant osteosarcoma stem cells, gavaged with β-elemene, and injected with lentiviral sh-NC), and the β-elemene + sh-FoxO1 group (injected with DOX-resistant osteosarcoma stem cells, gavaged with β-elemene, and injected with lentiviral sh-FoxO1). Once the tumor volume in each group reached approximately 100 mm^3, the Control group continued to receive normal saline via gavage, while the β-elemene-treated groups were administered 50 mg/kg of β-elemene *via* gavage every other day for two weeks. Lentiviruses (2×10^8 TU; sh-NC or sh-FoxO1) were injected *via* the tail vein once weekly [35–37]. Body weight was recorded weekly, and tumor diameters were measured using calipers to calculate tumor volume (longest diameter × shortest diameter^2 × 0.5). After 28 days, the mice were euthanized, tumor mass was recorded, and tumor tissues were collected for further experiments.

2.18. TUNEL staining

Paraffin sections were dewaxed and hydrated as previously described. Sections were immersed in 3 % hydrogen peroxide for 15 min, followed by incubation with Proteinase K (20 μg/ml in Tris/HCl) (ST535, Beyotime, China) at room temperature for 30 min. The sections were washed twice with PBS for 5 min each, with excess liquid blotted around the samples. TUNEL reaction mixture (C1086, Beyotime, China) was then applied, and sections were incubated in a humidified chamber at 37 °C for 60 min. After three washes in PBS, each lasting 5 min, nuclei were stained with DAPI (D8417, Sigma) and the slides were mounted. Apoptotic and total nuclei were visualized and quantified under a light microscope (XP-330, Shanghai Bingyu Optical Instruments, China) at 200x magnification.

2.19. Immunohistochemistry

Paraffin blocks were cooled on ice or refrigerated at 4 °C before sectioning. After drying overnight, slides were baked at 60 °C for 20 min. Sections were immersed in xylene for 10 min, refreshed with new xylene, and soaked for another 10 min. This was followed by rehydration in absolute ethanol for 5 min, refreshment, and another 5 min in absolute ethanol. Gradual rehydration was performed in 95 % and 70 % alcohol for 10 min each, then rinsed in distilled water for 5 min. Sections were then microwaved in citrate buffer (pH 6.0) for 1 min and cooled to room temperature. After three washes in PBS, each for 3 min, 3 % H_2O_2 was applied to quench endogenous peroxidase activity for 10 min at room temperature. This was followed by three PBS washes, each for 3 min. Normal goat serum (E510009, Sangon Biotech, Shanghai, China) was applied to block nonspecific binding at room temperature for 20 min. Sections were incubated overnight at 4 °C with primary antibodies against iNOS (ab178945, Abcam), CD86 (ab234000, Abcam), Arg1 (ab315110, Abcam), and CD206 (ab64693, Abcam). After overnight incubation, sections were washed three times in PBS, then incubated with 100 μL of polymer-conjugated goat anti-mouse/rabbit IgG (pv6000/pv9000, Zhongshan Golden Bridge, China) for 30 min. Color development was performed using a DAB Chromogen Kit (ZLI-9018, Zhongshan Golden Bridge, China) and examined under a microscope. Images were captured for documentation.

2.20. Statistical analysis

Data were derived from at least three independent experiments and are presented as mean ± standard deviation (Mean ± SD). For comparisons between the two groups, an independent samples *t*-test was employed. A one-way analysis of variance (ANOVA) was utilized for comparisons among three or more groups. If the ANOVA indicated significant differences, post hoc comparisons between groups were conducted using Tukey's HSD test. The Mann-Whitney *U* test or the Kruskal-Wallis H test was applied for data that were not normally distributed or had unequal variances. All statistical analyses were performed using GraphPad Prism 9 (GraphPad Software, Inc.) and R software. The significance level for all tests was set at 0.05, and a two-tailed *p*-value of less than 0.05 was considered statistically significant.

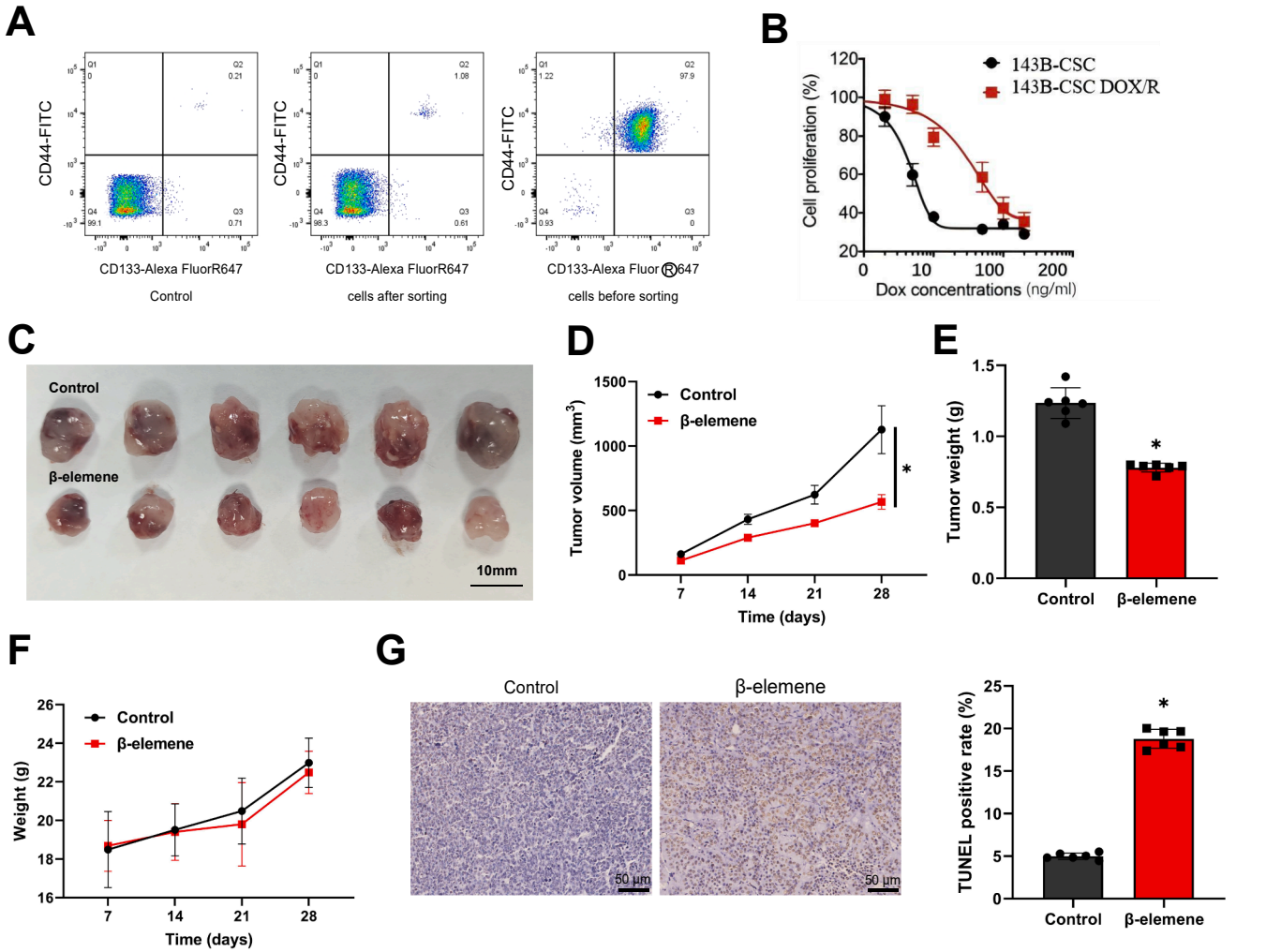

Fig. 1. Therapeutic effects of β-elemene on DOX-resistant osteosarcoma xenograft model. Note: (A) Flow cytometric isolation of osteosarcoma stem cells (CD44 + CD133 + cells); (B) CCK-8 assay assessing cell viability of osteosarcoma stem cells and DOX-resistant osteosarcoma stem cells treated with varying concentrations of DOX; (C) Tissue morphology of tumors from different mouse groups; (D) Statistical analysis of tumor volumes across different mouse groups; (E) Statistical analysis of tumor mass across different mouse groups; (F) Body weight statistics of mice in each group; (G) Detection and analysis of representative images of tumor tissues from each group of mice and the corresponding TUNEL-positive cell rates. * Indicates significant difference compared to the Control group, $p < 0.05$, n = 6 mice per group.

3. Results

3.1. Enhancement of DOX efficacy and reduction of osteosarcoma drug resistance by β-Elemene

β-Elemene, a plant-derived, non-cytotoxic anticancer agent, has been extensively studied recently [38]. Research indicates that β-elemene enhances the sensitivity of various cancer cells to multiple chemotherapy agents such as cisplatin, DOX, 5-fluorouracil (5-FU), paclitaxel, gefitinib, temozolomide, and docetaxel, thereby altering drug resistance and improving the anticancer efficacy of these chemotherapeutics [39]. However, no studies have yet reported whether β-elemene can enhance the sensitivity of osteosarcoma cells to DOX, reduce DOX resistance-related properties, and thus improve chemotherapy outcomes in osteosarcoma.

Our study cultured osteosarcoma cells and isolated osteosarcoma stem cells (CD44 + CD133 + cells) through flow cytometry (Fig. 1A and Fig. S1A). We then treated these cells with DOX to develop a DOX-resistant osteosarcoma stem cell line. Compared to the parent osteosarcoma stem cells, the DOX-resistant cells exhibited significantly increased resistance to DOX (Fig. 1B). In a xenograft model of DOX-resistant osteosarcoma in mice, we randomly assigned the animals to either a control or a β-elemene treatment group. Throughout the treatment period, we regularly measured the mice's tumor volume and body weight changes. Results indicated that tumor volumes and masses in the β-elemene group were significantly smaller than those in the control group (Fig. 1C-E). Additionally, there were no significant differences in body weight changes between groups, suggesting that the treatment regimen had minimal side effects (Fig. 1F).

At the end of the experiment, we extracted the mouse tumor tissues for TUNEL staining. The results showed that the apoptosis rate in the tumor cells from the β-elemene-treated group was significantly higher than in the DOX-treated group (Fig. 1G).

These findings suggest that β-elemene can inhibit the tumorigenic capacity of osteosarcoma stem cells *in vivo* and reduce the pro-tumor properties of DOX-resistant cells, thereby potentially enhancing the therapeutic efficacy of chemotherapy in osteosarcoma.

Identification of key pathogenic genes and signaling pathways in osteosarcoma with AKT1 identified as a core regulatory factor through WGCNA analysis

WGCNA is a pivotal tool in bioinformatics for identifying disease-causing genes by establishing co-expression networks from gene expression data, revealing molecular mechanisms associated with diseases, and is particularly significant for identifying key pathogenic genes [40]. To identify core genes crucial for the progression of osteosarcoma, we conducted a WGCNA on osteosarcoma-related genes and revealed key BP involved in its onset and progression. Utilizing the GEO database's osteosarcoma-related microarray GSE99671, which includes transcriptomic sequencing data sets from 18 osteosarcoma samples and 18 corresponding normal tissue samples, differential gene analysis yielded 3454 significantly DEGs (Fig. S1B). We retrieved a set of osteosarcoma-related disease targets from the GeneCards and Disgenet online databases to further identify genes that significantly impact osteosarcoma progression. By intersecting these targets with DEGs, we identified 740 disease target genes showing differential expression (Fig. S1C). Subsequently, using these selected target genes, we constructed a comprehensive gene co-expression network through WGCNA. The optimal soft thresholding power β\betaβ was calculated using R software and determined to be 8, fulfilling the scale-free network criterion (Fig. 2A). Based on this threshold, we set the minimum module size to 50 and a module merging threshold of 0.6 for dynamic tree cutting (Fig. 2B), which identified three gene modules: MEblue, MEturquoise, and MEgrey. Using these three clustered modules, we categorized normal and osteosarcoma samples based on clinical characteristics and analyzed the correlation between gene modules and clinical features. The results revealed that MEblue had the strongest correlation with osteosarcoma, with a correlation coefficient of −0.73 and a significance *p*-value of less than 0.001 (Fig. 2C).

GO/KEGG enrichment analysis of the 374 genes in MEblue revealed key biological pathways involved in osteosarcoma progression. The BP were predominantly enriched in the "immune system process" and "hematopoietic or lymphoid organ development," suggesting these genes play significant roles in immune regulation and development. CC was mainly enriched in the "extracellular region" and "cell surface," highlighting the importance of protein interactions and signal transduction in osteosarcoma progression. MF is closely related to "enzyme binding" and "transcription factor binding" and indicates potential involvement in regulating other protein activities or gene expression processes (Fig. S1D-F). Additionally, KEGG enrichment analysis revealed close associations with the PI3K-AKT signaling pathway, FOXO1 signaling pathway, and Pathways in cancer, suggesting these genes are crucial for cancer development and cellular survival signaling (Fig. S1G).

A PPI network for the module genes was constructed using the STRING online database to further refine the selection of core target genes. The centrality of each gene within this network was assessed based on their interactions. The results indicated that AKT1 had the highest centrality (Fig. 2D-E). AKT1 is one of three AKT isoforms in mammalian cells and is a crucial regulator of cell growth, proliferation, metabolism, and survival [41]. Studies show that activated AKT1 can phosphorylate FOXO1, causing its translocation from the nucleus to the cytoplasm, thereby inhibiting its transcriptional activity and preventing the expression of pro-apoptotic and cell cycle inhibitory genes. This regulatory mechanism is part of the cellular response to growth signals, where overactivation of AKT1 promotes tumor growth and anti-apoptotic capabilities, a phenomenon common in various cancers [42,43].

In conclusion, we identify AKT1 as a key core gene in the progression of osteosarcoma, potentially acting through the FOXO1 signaling pathway based on the KEGG enrichment results.

3.2. Characteristics of immune cell infiltration in osteosarcoma and the crucial role of M1 type macrophages

Immune cells play a critical role in osteosarcoma's development and treatment response. The activity and degree of infiltration of immune cells, such as T cells and macrophages, directly affect tumor growth, spread, and patient survival. These immune cells combat tumor invasion by recognizing and killing cancer cells or modulating the tumor microenvironment by releasing cytokines [44].

To elucidate the status of immune cell infiltration in osteosarcoma and identify key immune cells, we assessed the immune cell infiltration in osteosarcoma using the CIBERSORT algorithm. The results showed significant reductions in naive B cells, naive CD4 T cells, resting NK cells, eosinophils, and neutrophils in osteosarcoma samples compared to normal controls. In contrast, memory resting CD4 T cells, activated NK cells, and M1 type macrophages were significantly increased (Fig. 3A). These findings might reflect the impact of osteosarcoma on the immune system and its adaptive mechanisms. For instance, the reduction in naive B and T cells could indicate a deficiency in immune surveillance, while the increase in activated NK cells and M1 type macrophages suggests an attempt by the immune system to counteract the tumor [45].

We analyzed the correlations among immune cells to further identify immune cells critical for osteosarcoma progression. The results demonstrated strong interactions between macrophages and other immune cells, with significant correlations (Fig. 3B). Macrophages are multifunctional immune cells that maintain health primarily by phagocytosing pathogens, dead cells, and other debris. They are typically categorized into M1 and M2 types [46]. M1 type macrophages, with pro-inflammatory and antimicrobial properties, play roles in

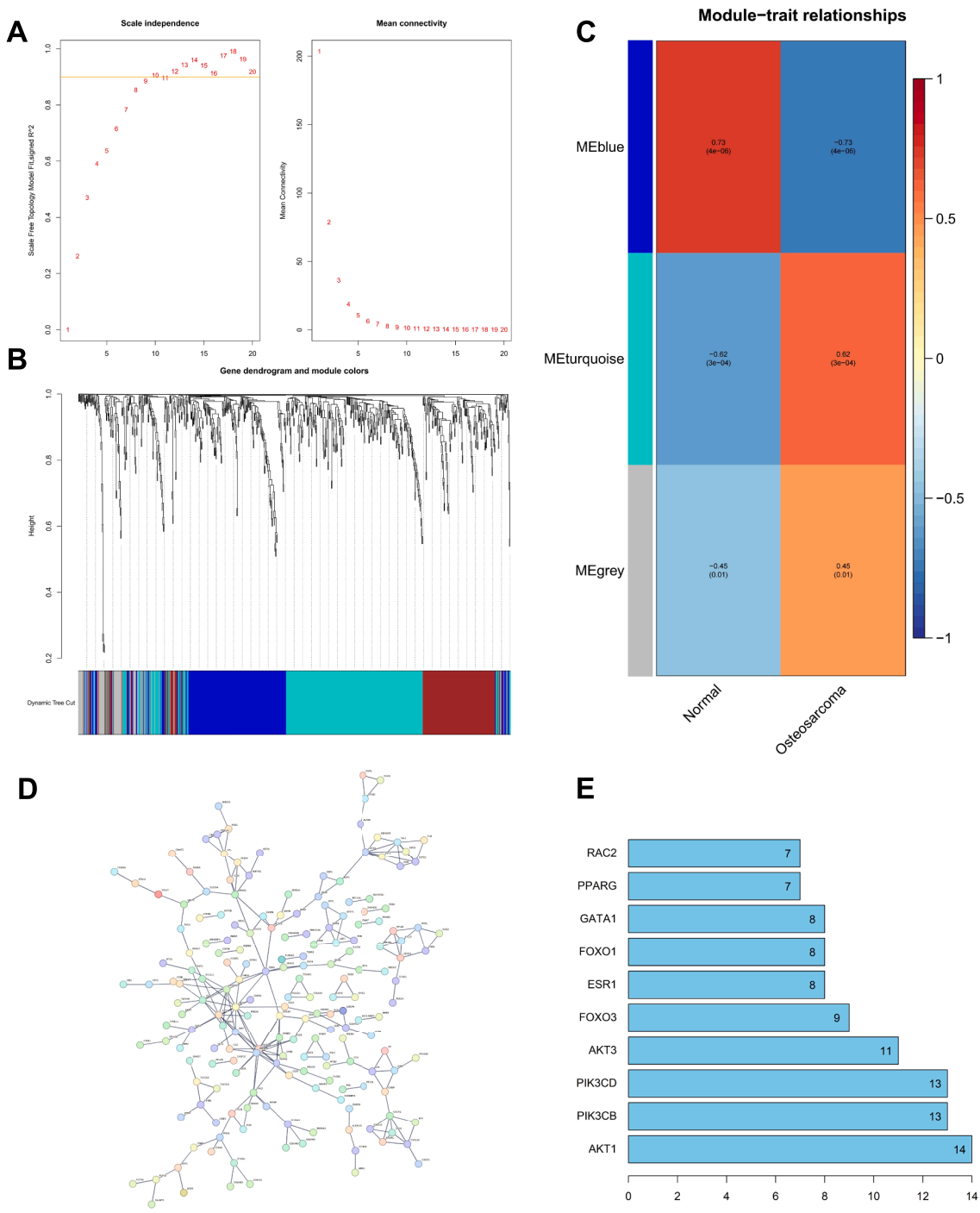

Fig. 2. WGCNA selection of key disease genes. Note: (A) Scale independence, mean connectivity, and scale-free topology plots, with a selected weighted value β = 8 to satisfy the scale-free network criterion; (B) Dendrogram of co-expression network modules; (C) Correlation between gene modules obtained through clustering and normal vs. osteosarcoma groups; (D) PPI network graph of the MEblue module factors; (E) Statistical chart of PPI network connectivity node counts for key candidate genes, where the horizontal axis represents the number of connectivity nodes—the higher the number, the higher the centrality. Sample size n = 18 for each group.

infections and tumors by producing inflammatory mediators like nitric oxide and pro-inflammatory cytokines, thereby enhancing immune responses. Conversely, M2 macrophages exhibit anti-inflammatory properties, are involved in tissue repair and healing, and modulate immune responses by producing anti-inflammatory cytokines and factors that promote tissue reconstruction [46]. Given the significant increase in Macrophages_M1 from our differential analysis, we hypothesize that M1 type macrophages are key immune cells involved in the progression of osteosarcoma.

The literature reports that AKT1 plays a significant role in regulating M1 type macrophages, for example, by promoting the expression of pro-inflammatory factors like TNF-α and IL-6 through activation of signaling pathways such as NF-κB, thereby influencing the survival, metabolic pathways, and functional activity of M1 type macrophages [47].

These results underscore that M1 type macrophages are key immune cells associated with osteosarcoma progression.

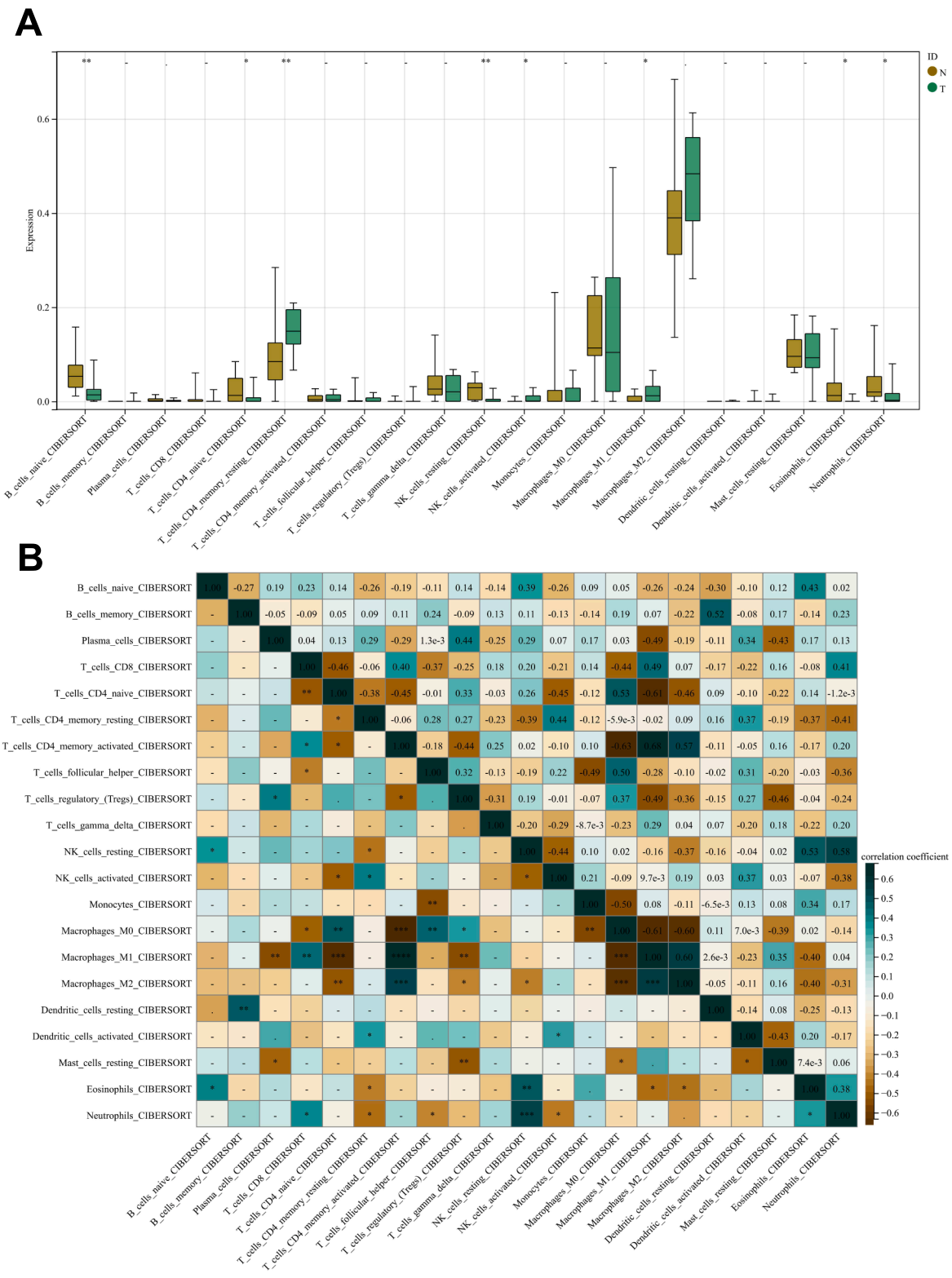

Fig. 3. Identification of key immune cells in the progression of osteosarcoma. Note: (A) Box plot showing immunological differences between normal and osteosarcoma groups; (B) Heatmap of intercellular correlations among immune cells. **** indicates $p < 0.0001$ compared to the normal group; *** indicates $p < 0.001$ compared to the normal group; ** indicates $p < 0.01$ compared to the normal group; * indicates $p < 0.05$ compared to the normal group. Sample size n = 18 for each group.

3.3. Inhibition of osteosarcoma progression by β-Elemene via Modulation of TP53 and AKT1 interaction mechanisms

We utilized network pharmacology approaches to identify potential targets for β-elemene in treating osteosarcoma. Initially, potential targets of β-elemene were predicted using the TCMSP and SWISS databases, resulting in 43 potential drug target genes after removing three duplicates (Fig. 4A). Subsequently, osteosarcoma-related genes from the GeneCards and Disgenet databases were consolidated, resulting in 5138 disease-related genes after removing 1722 duplicates (Fig. 4B). An

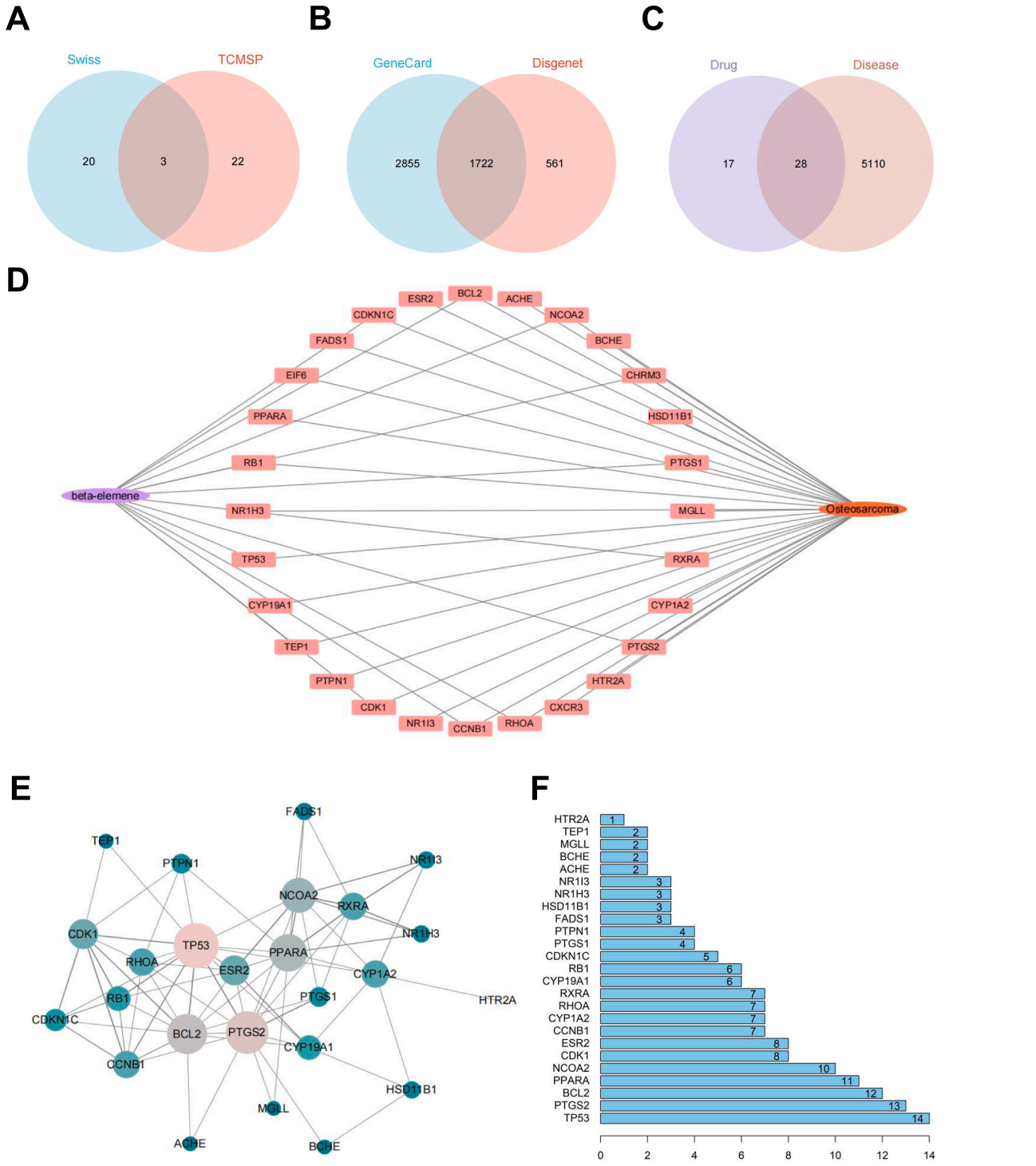

Fig. 4. Network pharmacology exploration of β-elemene's interaction with osteosarcoma and its potential key targets and mechanisms. Note: (A) Venn diagram of potential action targets of β-elemene identified through the SWISS and TCMSP databases; (B) Venn diagram identifying osteosarcoma-related target genes through online databases GeneCard and Disdenet; (C) Venn diagram of the intersection of disease-related targets with drug-related targets; (D) Network constructed in Cytoscape software showing β-elemene-target-disease interactions, with purple representing β-elemene, orange representing osteosarcoma, and pink representing potential therapeutic targets for osteosarcoma; (E) PPI network of 28 potential therapeutic targets constructed in Cytoscape software based on the STRING online database, with larger circles indicating a greater number of connectivity nodes; (F) Statistical chart of connectivity node counts for potential therapeutic target genes. (For interpretation of the references to color in this figure legend, the reader is referred to the web version of this article.)

intersection of drug target genes with disease-related genes yielded 28 potential targets for β-elemene treatment in osteosarcoma (Fig. 4C). These targets and their interactions with the drug were then mapped using Cytoscape to establish a network model of β-elemene components, targets, and disease pathways in treating osteosarcoma (Fig. 4D).

To uncover the potential molecular mechanisms or pathways through which β-elemene treats osteosarcoma, an enrichment analysis was conducted on these 28 potential targets. The results showed significant enrichment of BP, such as generation of precursor metabolites and energy and response to steroid hormone; CC, such as transcription regulator complex and nuclear periphery; MF, such as ligand-activated transcription factor activity and nuclear receptor activity; and key KEGG pathways, including Chemical carcinogenesis − receptor activation, Cell cycle, and p53 signaling pathway (Fig. S2A). These findings suggest that the genes may play a central role in cellular energy metabolism, hormone response, cell cycle control, and carcinogenic processes. Notably, significant enrichment in the p53 signaling pathway indicates their crucial role in cellular responses to DNA damage and tumor suppression. Furthermore, the functions highlighted in nuclear receptor activity and cell cycle regulation underscore the importance of these genes in regulating cell growth and differentiation.

Subsequently, we retrieved the protein interaction relationships for the 28 potential targets using the STRING online database. These interactions were visualized using Cytoscape software (Fig. 4E), and the connectivity of the genes was quantified using R software, resulting in a ranking based on the number of connection nodes. The results revealed that TP53 exhibited the highest centrality (Fig. 4F). TP53 (p53) primarily functions as a tumor suppressor, regulating the cell cycle, apoptosis, and genomic stability in response to cellular stressors such as DNA damage and oxidative stress [48]. Previous analyses identified AKT1 as a key pathogenic gene in osteosarcoma. To explore whether β-elemene could influence osteosarcoma treatment by affecting AKT1, we investigated the regulatory genes between TP53 and AKT1 using the Genemania online database. This investigation revealed 20 interacting genes, including PTEN, suggesting a regulatory effect of TP53 on AKT1 (Fig. S2B). Research has shown that p53 can indirectly affect the AKT signaling pathway, primarily through its downstream target PTEN, a phosphatidylinositol-3-kinase inhibitor, thereby influencing AKT activation [49,50].

These findings suggest that β-elemene may modulate osteosarcoma progression by regulating TP53, which affects PTEN and controls AKT1.

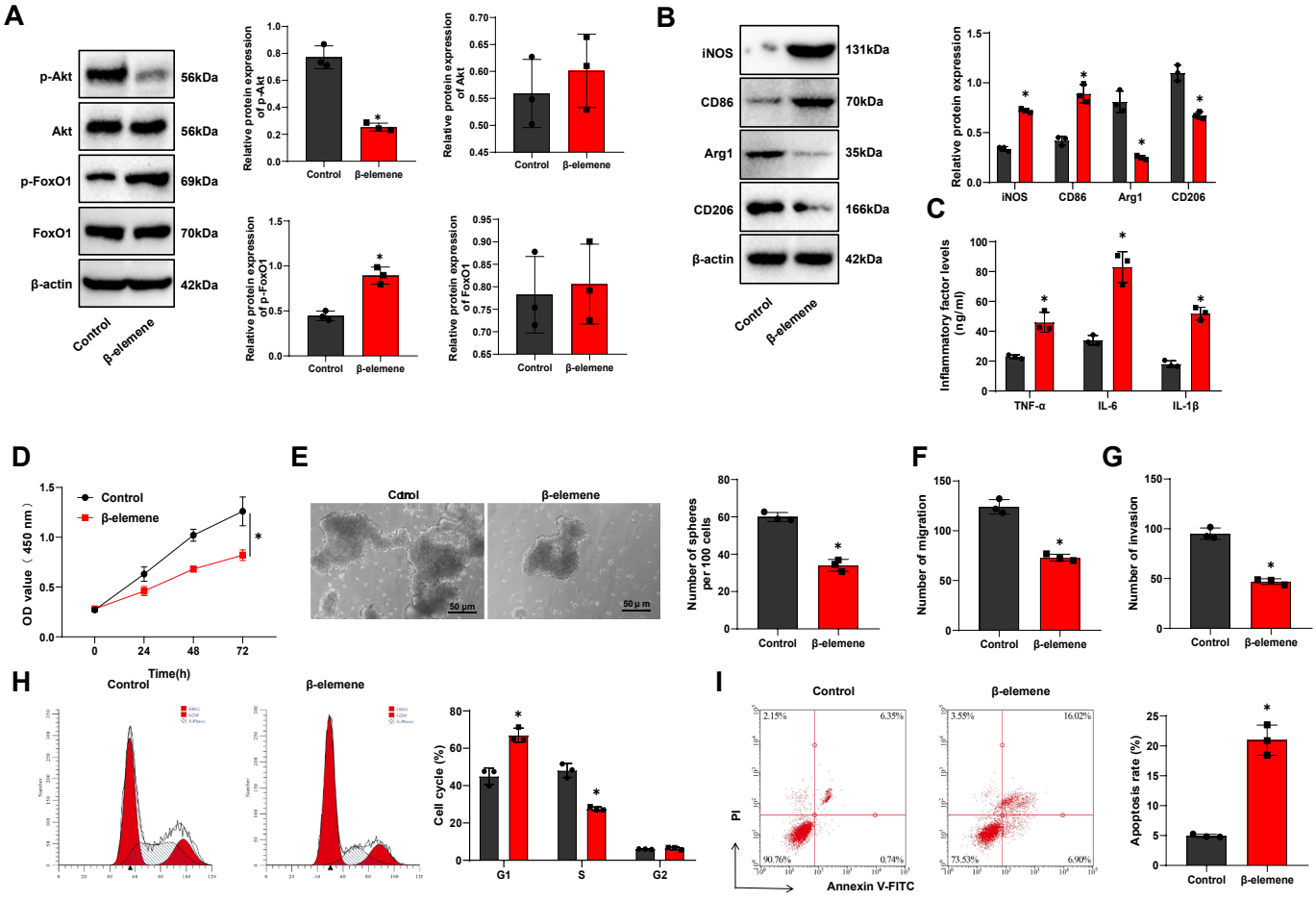

Fig. 5. β-elemene modulates AKT/FOXO1 signaling axis to activate M1 type macrophages and suppress drug resistance and stemness in osteosarcoma stem cells. Note: (A) WB analysis of p-AKT/AKT and p-FOXO1/FOXO1 expression levels in macrophages from each group; (B) WB analysis of M1 markers iNOS, CD86 and M2 markers Arg1, CD206 in macrophages from each group; (C) ELISA measurement of TNF-α, IL-6, and IL-1β levels in macrophages from each group; (D) CCK-8 assay to assess cell proliferation capability of DOX-resistant osteosarcoma stem cells co-cultured with macrophages; (E) Spheroid formation assay to evaluate the sphere-forming capability of DOX-resistant osteosarcoma stem cells co-cultured with macrophages (scale bar: 50 μm); (F) Transwell assay to assess cell migration ability of DOX-resistant osteosarcoma stem cells co-cultured with macrophages; (G) Transwell assay to evaluate cell invasion capability of DOX-resistant osteosarcoma stem cells co-cultured with macrophages; (H) Flow cytometry analysis of cell cycle distribution in DOX-resistant osteosarcoma stem cells co-cultured with macrophages; (I) Flow cytometry analysis of apoptosis rate in DOX-resistant osteosarcoma stem cells co-cultured with macrophages. * indicates a significant difference compared to the Control group, $p < 0.05$, with each cell experiment repeated three times.

3.4. β-Elemene reduces osteosarcoma stem cell stemness by promoting M1 Macrophage activation through inhibition of the Akt/FoxO1 signaling axis

Based on the aforementioned bioinformatics analysis, it is hypothesized that β-elemene promotes M1 macrophage polarization and inflammatory cytokine secretion via the Akt/FoxO1 signaling pathway, thereby affecting the drug resistance and stemness of osteosarcoma stem cells. To validate this hypothesis, we established a Control group and a β-elemene-treated group for macrophages.

Western blot results showed that, compared to the Control group, the β-elemene-treated group exhibited significantly reduced p-Akt levels and increased p-FoxO1 expression levels in macrophages (Fig. 5A). Additionally, the expression of M1 markers iNOS and CD86 was significantly increased, while the expression of M2 markers Arg1 and CD206 was significantly decreased in the β-elemene-treated group (Fig. 5B). ELISA results further demonstrated that the secretion levels of TNF-α, IL-6, and IL-1β were significantly elevated in the β-elemene-treated group (Fig. 5C), indicating that β-elemene effectively promotes M1 macrophage polarization.

In a co-culture system, β-elemene-treated macrophages were cultured with drug-resistant osteosarcoma stem cells. The CCK-8 assay revealed that the survival rate of osteosarcoma stem cells was significantly reduced in the β-elemene-treated group (Fig. 5D). Tumor sphere formation assays showed a significant reduction in the number of tumor spheres in the β-elemene-treated group (Fig. 5E), suggesting that β-elemene suppresses the stemness of osteosarcoma stem cells. Transwell migration and invasion assays demonstrated that the migration and invasion abilities of osteosarcoma stem cells were significantly decreased in the β-elemene-treated group (Fig. 5F-G). These findings indicate that β-elemene promotes M1 macrophage polarization through the Akt/FoxO1 signaling pathway, thereby reducing the drug resistance and stemness of osteosarcoma stem cells.

Flow cytometric analysis of cell cycle distribution and apoptosis rates further confirmed these results. In the β-elemene-treated group, the proportion of osteosarcoma stem cells in the G1 phase significantly increased, while the proportion in the S phase significantly decreased (Fig. 5H). Additionally, the apoptosis rate of osteosarcoma stem cells was significantly elevated in the β-elemene-treated group (Fig. 5I). These results provide further evidence that β-elemene inhibits the Akt/FoxO1 signaling pathway, promoting M1 macrophage polarization and inflammatory cytokine secretion, thereby significantly reducing the drug resistance and stemness of osteosarcoma stem cells.

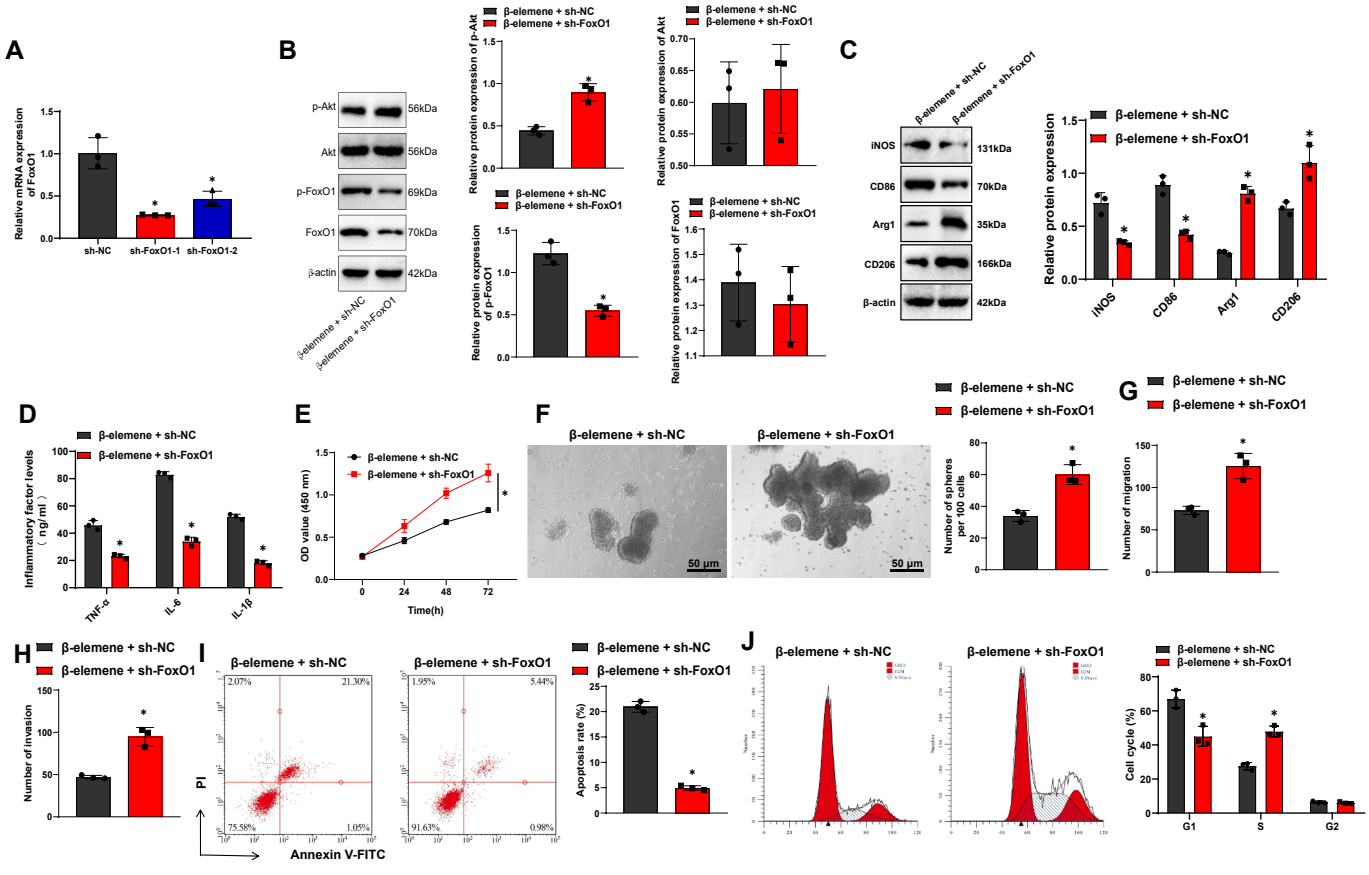

Fig. 6. Reversal of β-elemene-induced activation of M1 type macrophages by silencing FOXO1 enhances drug resistance and stemness in osteosarcoma stem cells. Note: (A) qRT-PCR analysis of the silencing efficiency of sh-FOXO1; (B) WB analysis of p-AKT/AKT and p-FOXO1/FOXO1 expression levels in macrophages from each group; (C) WB analysis of the expression of M1 markers (iNOS, CD86) and M2 markers (Arg1, CD206) in macrophages from each group; (D) ELISA measurement of TNF-α, IL-6, and IL-1β levels in macrophages from each group; (E) CCK-8 assay to assess cell proliferation capability of DOX-resistant osteosarcoma stem cells co-cultured with macrophages; (F) Spheroid formation assay to evaluate the sphere-forming capability of DOX-resistant osteosarcoma stem cells co-cultured with macrophages (scale bar: 50 μm); (G) Transwell assay to assess cell migration ability of DOX-resistant osteosarcoma stem cells co-cultured with macrophages; (H) Transwell assay to evaluate cell invasion capability of DOX-resistant osteosarcoma stem cells co-cultured with macrophages; (I) Flow cytometry analysis of apoptosis rate in DOX-resistant osteosarcoma stem cells co-cultured with macrophages; (J) Flow cytometry analysis of cell cycle distribution in DOX-resistant osteosarcoma stem cells co-cultured with macrophages. * indicates a significant difference compared to the sh-NC group or β-elemene + sh-NC group, $p < 0.05$, with each cell experiment repeated three times.

3.5. The silencing of FoxO1 reverses β-elemene-induced M1 macrophage activation and promotes the stemness of osteosarcoma stem cells

The above *in vitro* experimental results demonstrate that β-elemene inhibits the Akt/FoxO1 signaling axis, promoting M1 macrophage polarization and inflammatory cytokine secretion, thereby significantly reducing the drug resistance and stemness of osteosarcoma stem cells. To further validate this regulatory mechanism, we silenced FoxO1 in macrophages and treated them with β-elemene.

First, the silencing efficiency of sh-FoxO1 was evaluated using qRT-PCR. Results showed that both sh-FoxO1-1 and sh-FoxO1-2 significantly reduced FoxO1 expression compared to sh-NC (Fig. 6A). Based on the superior silencing effect of sh-FoxO1-1, it was selected for subsequent experiments and referred to as sh-FoxO1.

Western blot results revealed that, compared to the β-elemene + sh-NC group, the β-elemene + sh-FoxO1 group exhibited significantly increased p-Akt levels and significantly reduced p-FoxO1 and FoxO1 expression levels in macrophages (Fig. 6B). Additionally, in the β-elemene + sh-FoxO1 group, the expression of M1 markers iNOS and CD86 was significantly decreased, while the expression of M2 markers Arg1 and CD206 was significantly increased compared to the β-elemene + sh-NC group (Fig. 6C). ELISA results further demonstrated that the secretion levels of TNF-α, IL-6, and IL-1β were significantly reduced in the β-elemene + sh-FoxO1 group compared to the β-elemene + sh-NC group (Fig. 6D). These findings indicate that FoxO1 silencing reverses β-elemene-induced promotion of M1 macrophage polarization.

In a co-culture system, macrophages treated with both β-elemene and sh-FoxO1 were co-cultured with drug-resistant osteosarcoma stem cells. CCK-8 assay results showed that the survival rate of osteosarcoma stem cells was significantly increased in the β-elemene + sh-FoxO1 group compared to the β-elemene + sh-NC group (Fig. 6E). Tumor sphere formation assays indicated that the number of tumor spheres significantly increased in the β-elemene + sh-FoxO1 group compared to the β-elemene + sh-NC group (Fig. 6F). Transwell migration and invasion assays revealed that osteosarcoma stem cells co-cultured with macrophages in the β-elemene + sh-FoxO1 group exhibited significantly enhanced migration and invasion abilities compared to those in the β-elemene + sh-NC group (Fig. 6G-H).

Flow cytometric analysis of apoptosis and cell cycle distribution further confirmed these findings. The apoptosis rate of osteosarcoma stem cells co-cultured with macrophages in the β-elemene + sh-FoxO1 group was significantly reduced compared to the β-elemene + sh-NC group (Fig. 6I). The proportion of cells in the G1 phase was significantly reduced, while the proportion in the S phase was significantly increased in the β-elemene + sh-FoxO1 group compared to the β-elemene + sh-NC group (Fig. 6J).

These results indicate that the silencing of FoxO1 reverses β-elemene-induced promotion of M1 macrophage polarization, thereby promoting the drug resistance and stemness of osteosarcoma stem cells.

3.6. β-Elemene reduces osteosarcoma resistance by promoting M1 macrophage activation through inhibition of the Akt/FoxO1 signaling axis

In the DOX-resistant osteosarcoma xenograft mouse model, animals were divided into four groups: Control, β-elemene, β-elemene + sh-NC, and β-elemene + sh-FoxO1. During the four treatment cycles, tumor volumes and body weight changes were measured regularly. Results showed that tumor volumes and masses were significantly increased in the β-elemene + sh-FoxO1 group compared to the β-elemene + sh-NC group (Fig. 7A-C). Additionally, there were no significant differences in body weight changes across groups, indicating that the treatment regimens had no apparent toxic side effects (Fig. 7D).

At the end of the experiment, tumor tissues were collected for Western blot analysis. Compared to the Control group, the β-elemene group exhibited significantly reduced p-Akt levels and increased p-FoxO1 levels in tumor tissues. In contrast, the β-elemene + sh-FoxO1 group showed significantly increased p-Akt levels and reduced p-FoxO1 levels compared to the β-elemene + sh-NC group (Fig. 7E).

Immunohistochemistry results revealed that, compared to the Control group, the β-elemene group had significantly increased expression of M1 macrophage markers iNOS and CD86 and significantly decreased expression of M2 macrophage markers Arg1 and CD206 in tumor tissues. However, compared to the β-elemene + sh-NC group, the β-elemene + sh-FoxO1 group exhibited significantly reduced expression of M1 markers iNOS and CD86 and increased expression of M2 markers Arg1 and CD206 (Fig. 7F).

ELISA results showed that inflammatory cytokines TNF-α, IL-6, and IL-1β levels were significantly elevated in tumor tissues of the β-elemene group compared to the Control group. Conversely, these cytokine levels were significantly decreased in the β-elemene + sh-FoxO1 group compared to the β-elemene + sh-NC group (Fig. 7G).

Further Western blot analysis revealed that stemness-related markers Oct4, Sox2, and Nanog were significantly reduced in the β-elemene group compared to the Control group. However, their expression was significantly increased in the β-elemene + sh-FoxO1 group compared to the β-elemene + sh-NC group (Fig. 7H).

These findings demonstrate that β-elemene reduces the drug resistance and stemness of osteosarcoma stem cells by inhibiting the Akt/FoxO1 signaling axis, promoting M1 macrophage polarization, and enhancing inflammatory cytokine secretion.

4. Discussion

β-Elemene, a natural monoterpene compound, has shown extensive potential in cancer therapy. Numerous studies have demonstrated that β-elemene can inhibit tumor cell proliferation, induce apoptosis, and modulate the tumor immune microenvironment by regulating signaling pathways such as PI3K/Akt and NF-κB, thereby influencing tumor cell biological behavior [51–53]. Although β-elemene has shown significant therapeutic effects in various tumors, its application in osteosarcoma remains relatively underexplored [54,55]. This study is the first to reveal that β-elemene activates macrophage-mediated immune responses through the Akt/FoxO1 signaling pathway, providing novel theoretical support for its potential application in osteosarcoma treatment.

The Akt/FoxO1 signaling pathway is a key intracellular regulatory axis involved in cell survival, proliferation, apoptosis, and immune regulation. Akt activation suppresses the transcriptional inhibitory function of FoxO1, thereby modulating immune cell functions and altering the tumor microenvironment composition [56]. In the tumor immune microenvironment, the Akt/FoxO1 pathway regulates the activity of macrophages, T cells, and natural killer cells, directly affecting immune escape mechanisms and drug resistance [57,58]. By inhibiting the Akt/FoxO1 axis, β-elemene promotes M1 macrophage polarization and enhances their anti-tumor activity, while suppressing osteosarcoma stem cell drug resistance and stemness. Tumor-associated macrophages play a critical role in the progression and regulation of osteosarcoma. M1 macrophages, through the secretion of inflammatory cytokines such as TNF-α and IL-1, directly kill tumor cells, whereas M2 macrophages promote tumor growth, invasion, and immune escape [59,60].

In this study, β-elemene significantly enhanced the activity of M1 macrophages, as evidenced by increased expression of M1 markers iNOS and CD86, decreased expression of M2 markers Arg1 and CD206, and elevated levels of inflammatory cytokines TNF-α, IL-6, and IL-1β. This immune polarization inhibited osteosarcoma stem cell stemness and resistance, effectively reducing their survival and tumorigenic capacity. These findings underscore the potential of β-elemene in modulating immune cell function and suggest that β-elemene's anti-tumor effects are achieved, at least in part, through altering the macrophage polarization state. These results contrast with previous studies highlighting the pro-tumor role of macrophages, emphasizing the therapeutic significance of immune microenvironment polarization.

Osteosarcoma is a highly aggressive malignancy characterized by

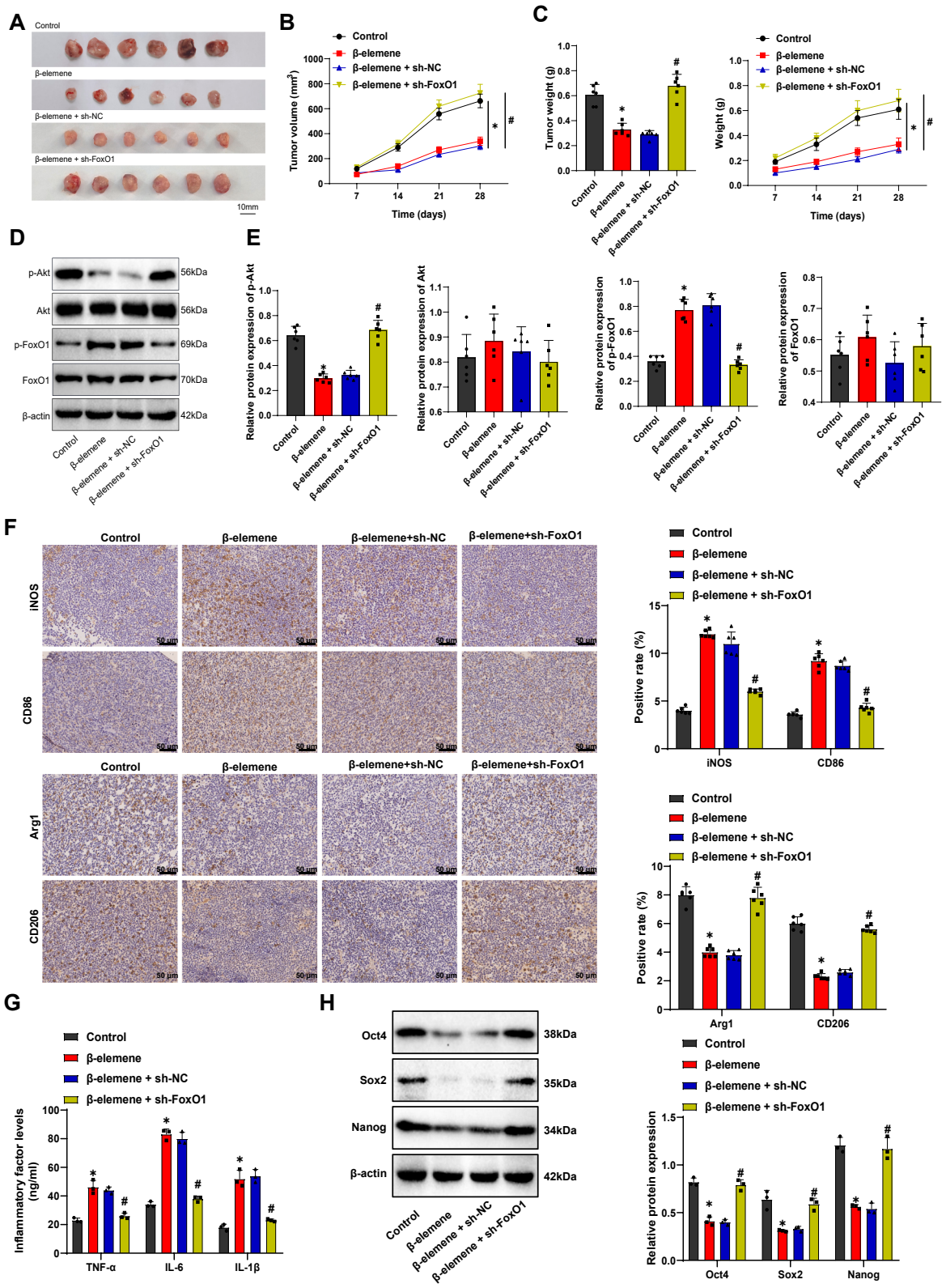

Fig. 7. Impact of β-elemene activating M1 type macrophages through the AKT/FOXO1 signaling axis on DOX-resistant osteosarcoma. Note: (A) Tumor tissue morphology of each mouse group; (B) Statistical analysis of tumor volume in each mouse group; (C) Statistical analysis of tumor mass in each mouse group; (D) Body weight statistics of each mouse group; (E) WB analysis of p-AKT/AKT and p-FOXO1/FOXO1 protein levels in tumor tissues of each mouse group; (F) Immunohistochemical staining showing expression of M1 markers iNOS, CD86, and M2 markers Arg1, CD206 in tumor tissues of each mouse group (scale bar: 50 μm); (G) ELISA measurement of inflammatory cytokines TNF-α, IL-6, and IL-1β in tumor tissues of each mouse group; (H) WB analysis of stemness-related markers Oct4, Sox2, and Nanog protein expression in mouse tumor tissues. * indicates a significant difference compared to the Control group, $p < 0.05$. # indicates significant difference compared to the β-elemene + sh-NC group, $p < 0.05$. n = 6 mice per group.

rapid growth, invasive behavior, and a propensity for metastasis. Despite advances in surgical techniques and chemotherapy, drug resistance remains a significant challenge, often leading to poor clinical outcomes [10,61]. Overcoming drug resistance has become a critical goal in osteosarcoma research. The tumor immune microenvironment, particularly the regulation of immune cell functions, has been increasingly recognized as a promising target for overcoming resistance. β-Elemene presents a novel approach by activating M1 macrophages and modulating the tumor microenvironment, ultimately reducing the stemness and resistance of osteosarcoma stem cells. These findings provide new insights into potential therapeutic strategies that target the tumor immune microenvironment to improve treatment efficacy in osteosarcoma.

This study employs a comprehensive approach, integrating bioinformatics analysis, *in vitro* experiments, and *in vivo* validation, to explore the mechanism of β-elemene in regulating macrophage activity and suppressing osteosarcoma resistance. By combining molecular pathway analysis with biological validation, the study offers a multidisciplinary perspective on the therapeutic potential of β-elemene. However, certain limitations should be acknowledged. For instance, the bioinformatics analysis may be affected by data quality and availability, while the animal models used may not fully replicate the complexity of human osteosarcoma. Furthermore, although the study demonstrates significant anti-tumor effects of β-elemene in animal models, further clinical validation is required to confirm its efficacy and safety in humans. Future research should focus on clinical trials to evaluate β-elemene's therapeutic potential and explore its application in other tumor types. Additionally, the potential synergistic effects of β-elemene with other immunotherapeutic agents warrant further investigation. These efforts could expand the application of β-elemene in cancer therapy and provide new treatment options for patients.

5. Conclusion

This study elucidates the mechanism by which β-elemene inhibits the stemness of osteosarcoma stem cells and reduce the pro-tumor characteristics of DOX-resistant osteosarcoma cells by suppressing the AKT/FOXO1 signaling pathway and activating a macrophage-mediated inflammatory microenvironment (Fig. 8). Both *in vivo* and *in vitro* experiments demonstrate that β-elemene treatment significantly lowers the survival rate of drug-resistant osteosarcoma cells, inhibits their stemness and migratory/invasive capabilities, and enhances anti-tumor immune responses by promoting M1 type macrophage polarization and increasing the secretion of inflammatory cytokines. These findings provide new potential targets and strategies for treating osteosarcoma resistance.

The scientific value of this research lies in revealing the specific molecular mechanisms by which β-elemene reverses resistance in osteosarcoma, offering fresh insights into the drug resistance of osteosarcoma stem cells. Clinically, as a natural compound with lower toxicity, β-elemene could become an effective and safe adjunct therapy for osteosarcoma. When used with existing chemotherapy drugs, β-elemene can improve treatment outcomes, enhance the quality of life, and extend survival for patients with osteosarcoma. Despite these insights into β-elemene's anti-tumor mechanisms, there are still limitations to this study. Primarily, the research was conducted in animal models and cell cultures, necessitating further clinical trials to confirm its safety and efficacy before clinical application. Additionally, the therapeutic effects of β-elemene on other types of tumors remain unclear, and further research is needed to explore its mechanisms across different cancers. Future research should focus on the clinical translation of β-elemene, optimizing its dosage and administration, and investigating its synergistic effects with other anti-cancer drugs. Furthermore, studies should

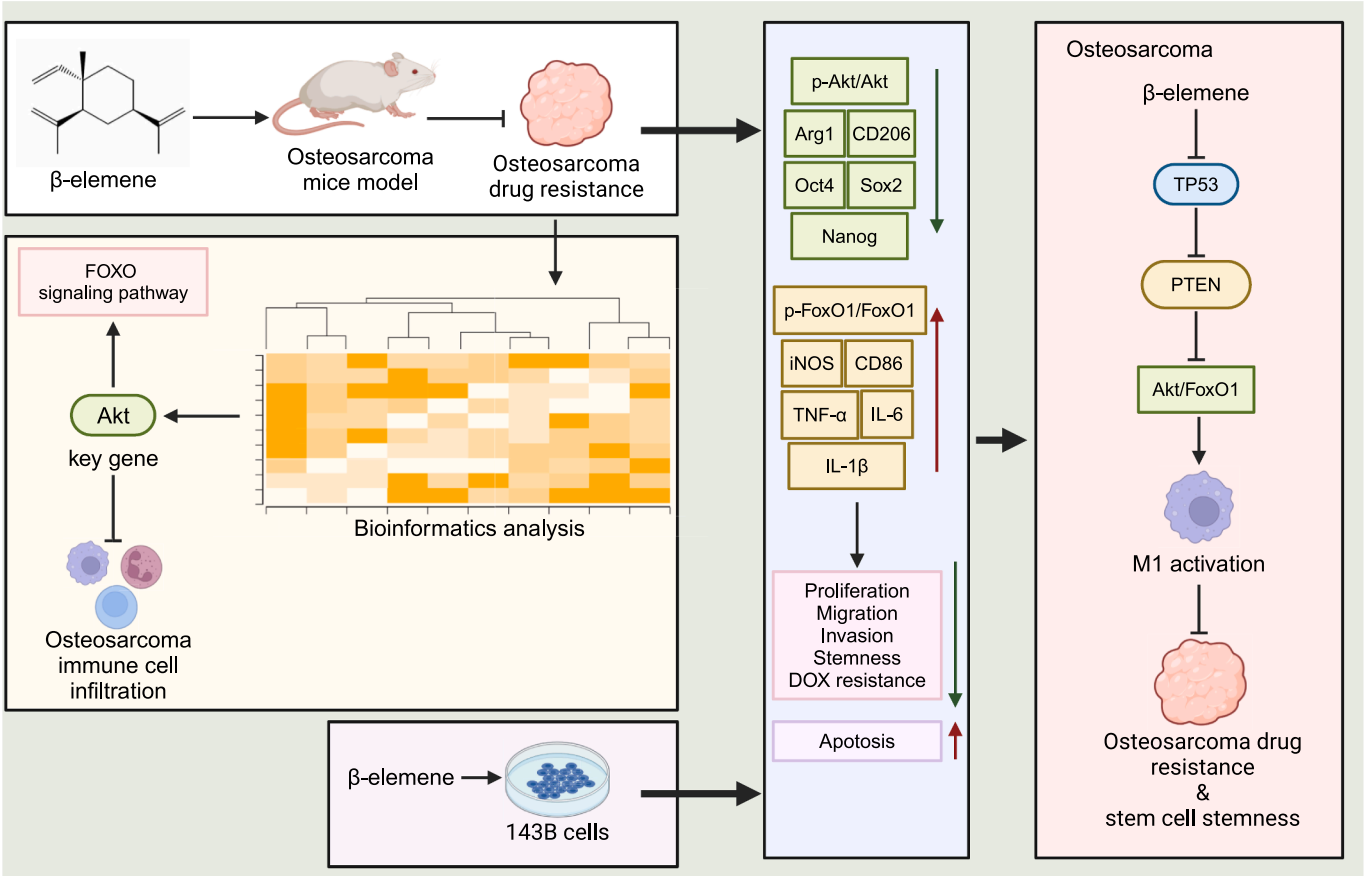

Fig. 8. Molecular mechanism of β-elemene in inhibiting osteosarcoma drug resistance.

explore its potential roles in other tumor microenvironments to expand its applicational scope.

Funding

This study was supported by the Natural Science Foundation of Hubei Province, No. 2022CFB077.

Ethics approval and consent to participate

All animal experiments were approved by the Animal Ethics Committee of The Central Hospital of Ezhou (Approval No. L2022-K-05). This study does not involve any human clinical trials or clinical ethics.

Availability of data and materials

All relevant data generated or analyzed during this study are included in this article. Further inquiries can be directed to the corresponding author.

CRediT authorship contribution statement

Shaochun Zhang: Writing – review & editing, Writing – original draft, Visualization, Validation, Project administration, Methodology, Investigation, Conceptualization. **Zhijie Xing:** Writing – original draft, Software, Resources, Methodology, Investigation, Conceptualization. **Jing Ke:** Writing – original draft, Visualization, Validation, Methodology, Investigation, Formal analysis.

Declaration of competing interest

The authors declare that they have no known competing financial interests or personal relationships that could have appeared to influence the work reported in this paper.

Appendix A. Supplementary data

Supplementary data to this article can be found online at https://doi.org/10.1016/j.jbo.2024.100655.

References

[1] N. Gaspar, Q. Campbell-Hewson, J. Huang, C.E. Okpara, F. Bautista, OLIE, ITCC-082: a phase II trial of lenvatinib plus ifosfamide and etoposide in relapsed/refractory osteosarcoma, Future Oncol. 17 (32) (2021) 4249–4261, https://doi.org/10.2217/fon-2021-0743.

[2] S.M. Gill, S. Mufty, A. Hassan, Spectrum of technetium-99m methylene diphosphonate (99mTc MDP) uptake in osteosarcoma, J. Pak. Med. Assoc. 73 (7) (2023) 1551–1552, https://doi.org/10.47391/JPMA.23-53.

[3] H. Tang, J. Xie, Y.X. Du, Z.J. Tan, Z.T. Liang, Osteosarcoma neutrophil extracellular trap network-associated gene recurrence and metastasis model. J. Cancer Res. Clin. Oncol. 2024;150(2):48. Published 2024 Jan 29. doi:10.1007/s00432-023-05577-2.

[4] J. Gotta, K. Bochennek, T. Klingebiel, et al., Metachronous osteosarcoma, a differential diagnosis to be considered in children with osteosarcoma: a review of literature and a case from our center, J. Pediatr. Hematol. Oncol. 45 (3) (2023) 105–110, https://doi.org/10.1097/MPH.0000000000002560.

[5] L. Tang, B. Liu, Lung and bone metastases patterns in osteosarcoma: chemotherapy improves overall survival, Medicine (Baltimore) 102 (4) (2023) e32692, https://doi.org/10.1097/MD.0000000000032692.

[6] D.J. Ho, N.P. Agaram, M.H. Jean, et al., Deep learning-based objective and reproducible osteosarcoma chemotherapy response assessment and outcome prediction, Am. J. Pathol. 193 (3) (2023) 341–349, https://doi.org/10.1016/j.ajpath.2022.12.004.

[7] C. Chen, S. Wang, J. Wang, F. Yao, X. Tang, W. Guo, Nanosized drug delivery strategies in osteosarcoma chemotherapy, APL Bioeng. 7 (1) (2023) 011501, https://doi.org/10.1063/5.0137026. Published 2023 Feb 23.

[8] G. Hu, D. Wang, Analysis of cardiac adverse reactions caused by different doses of adriamycin chemotherapy in patients with breast cancer. J. Healthc. Eng. 2022; 2022:1642244. Published 2022 Feb 15. doi:10.1155/2022/1642244.

[9] R.A. Gudur, S.J. Bhosale, A.K. Gudur, S.R. Kale, A.L. More, K.D. Datkhile, Influence of (C1236T and C3435T) polymorphisms of ABCB1 gene on chemotherapy treatment outcome and toxicity in breast cancer patients, Asian Pac. J. Cancer Prev. 25 (5) (2024) 1567–1577, https://doi.org/10.31557/APJCP.2024.25.5.1567. Published 2024 May 1.

[10] I. Panez-Toro, J. Muñoz-García, J.W. Vargas-Franco, et al., Advances in osteosarcoma, Curr. Osteoporos. Rep. 21 (4) (2023) 330–343, https://doi.org/10.1007/s11914-023-00803-9.

[11] X. Yang, S. Gao, B. Yang, et al., Bioinspired tumor-targeting and biomarker-activatable cell-material interfacing system enhances osteosarcoma treatment via biomineralization, Adv. Sci. (Weinh). 10 (22) (2023) e2302272, https://doi.org/10.1002/advs.202302272.

[12] Z. Tang, Y. Lu, Y. Chen, J. Zhang, Z. Chen, Q. Wang, Research progress of MicroRNA in chemotherapy resistance of osteosarcoma, Technol. Cancer Res. Treat. 20 (2021) 15330338211034262, https://doi.org/10.1177/15330338211034262.

[13] B. Wu, P. Li, E. Qiu, J. Chen, Metformin alleviates adriamycin resistance of osteosarcoma by declining YY1 to inhibit MDR1 transcriptional activity. BMC Pharmacol. Toxicol. 2023;24(1):50. Published 2023 Oct 12. doi:10.1186/s40360-023-00685-8.

[14] J. Gill, R. Gorlick, Advancing therapy for osteosarcoma, Nat. Rev. Clin. Oncol. 18 (10) (2021) 609–624, https://doi.org/10.1038/s41571-021-00519-8.

[15] D.P. Regan, L. Chow, S. Das, et al., Losartan blocks osteosarcoma-elicited monocyte recruitment, and combined with the kinase inhibitor toceranib, exerts significant clinical benefit in canine metastatic osteosarcoma, Clin. Cancer Res. 28 (4) (2022) 662–676, https://doi.org/10.1158/1078-0432.CCR-21-2105.

[16] H. Lin, X. Chen, C. Zhang, et al., EF24 induces ferroptosis in osteosarcoma cells through HMOX1, Biomed. Pharmacother. 136 (2021) 111202, https://doi.org/10.1016/j.biopha.2020.111202.

[17] R.P. Dos Santos, R. Roesler, L. Gregianin, et al., Cancer stem cells and chemoresistance in ewing sarcoma, Curr. Stem Cell Res. Ther. 18 (7) (2023) 926–936, https://doi.org/10.2174/1574888X17666220627114710.

[18] F. Moosavi, E. Giovannetti, G.J. Peters, O. Firuzi, Combination of HGF/MET-targeting agents and other therapeutic strategies in cancer, Crit. Rev. Oncol. Hematol. 160 (2021) 103234, https://doi.org/10.1016/j.critrevonc.2021.103234.

[19] H. Mo, R. Jeter, A. Bachmann, S.T. Yount, C.L. Shen, H. Yeganehjoo, The potential of isoprenoids in adjuvant cancer therapy to reduce adverse effects of statins, Front. Pharmacol. 9 (2019) 1515, https://doi.org/10.3389/fphar.2018.01515. . Published 2019 Jan 4.

[20] H.W. Dong, K. Wang, X.X. Chang, et al., Beta-ionone-inhibited proliferation of breast cancer cells by inhibited COX-2 activity, Arch. Toxicol. 93 (10) (2019) 2993–3003, https://doi.org/10.1007/s00204-019-02550-2.

[21] M.L.P. Miranda, K.S. Furtado, A.F. de Oliveira, et al., β-ionone inhibits nonalcoholic fatty liver disease and its association with hepatocarcinogenesis in male Wistar rats, Chem. Biol. Interact. 308 (2019) 377–384, https://doi.org/10.1016/j.cbi.2019.05.046.

[22] K. Aihaiti, J. Li, N.N. Xu, D. Tang, H.A. Aisa, Monoterpenoid derivatives from Hyssopus cuspidatus Boriss. and their bioactivities, Fitoterapia 165 (2023) 105432, https://doi.org/10.1016/j.fitote.2023.105432.

[23] M.A.A. Orabi, E.A. Orabi, A.A.A. Awadh, et al. New megastigmane and polyphenolic components of henna leaves and their tumor-specific cytotoxicity on human oral squamous carcinoma cell lines. Antioxidants (Basel). 2023;12(11): 1951. Published 2023 Nov 1. doi:10.3390/antiox12111951.

[24] S.W. Yue, H.L. Liu, H.F. Su, et al. m6A-regulated tumor glycolysis: new advances in epigenetics and metabolism. Mol. Cancer. 2023;22(1):137. Published 2023 Aug 15. doi:10.1186/s12943-023-01841-8.

[25] J. Liu, S.S. Liew, J. Wang, K. Pu, Bioinspired and biomimetic delivery platforms for cancer vaccines, Adv. Mater. 34 (1) (2022) e2103790, https://doi.org/10.1002/adma.202103790.

[26] C. Jiang, N. Zhang, X. Hu, H. Wang, Tumor-associated exosomes promote lung cancer metastasis through multiple mechanisms. Mol. Cancer. 2021;20(1):117. Published 2021 Sep 13. doi:10.1186/s12943-021-01411-w.

[27] J. Sun, Z. Liao, Z. Li, et al., Down-regulation miR-146a-5p in Schwann cell-derived exosomes induced macrophage M1 polarization by impairing the inhibition on TRAF6/NF-κB pathway after peripheral nerve injury, Exp. Neurol. 362 (2023) 114295, https://doi.org/10.1016/j.expneurol.2022.114295.

[28] L. Zhang, J. Zhao, X. Hu, et al., A peritumorally injected immunomodulating adjuvant elicits robust and safe metalloimmunotherapy against solid tumors, Adv. Mater. 34 (41) (2022) e2206915, https://doi.org/10.1002/adma.202206915.

[29] A. Karger, S. Mansouri, M.S. Leisegang, et al., ADPGK-AS1 long noncoding RNA switches macrophage metabolic and phenotypic state to promote lung cancer growth, EMBO J. 42 (18) (2023) e111620, https://doi.org/10.15252/embj.2022111620.

[30] Y. Hu, L. Han, W. Xu, et al., CARD11 regulates the thymic Treg development in an NF-κB-independent manner, Front. Immunol. 15 (2024) 1364957, https://doi.org/10.3389/fimmu.2024.1364957. . Published 2024 Apr 8.

[31] C.H. Chen, Y.C. Chen, Y.C. Chang, et al., Taurine rescues cancer-induced atrophy in human skeletal muscle cells via ameliorating the inflammatory tumor microenvironment, Anticancer Res 44 (5) (2024) 1963–1971, https://doi.org/10.21873/anticanres.16999.

[32] Z. Wei, K. Xia, D. Zheng, C. Gong, W. Guo, RILP inhibits tumor progression in osteosarcoma via Grb10-mediated inhibition of the PI3K/AKT/mTOR pathway. Mol. Med. 2023;29(1):133. Published 2023 Oct 3. doi:10.1186/s10020-023-00722-6.

[33] S.V. Tsang, N. Rainusso, M. Liu, et al., LncRNA PVT-1 promotes osteosarcoma cancer stem-like properties through direct interaction with TRIM28 and TSC2 ubiquitination, Oncogene 41 (50) (2022) 5373–5384, https://doi.org/10.1038/s41388-022-02538-w.

[34] L. Fang, B. Wang, Z. Yang, T. Zhao, W. Hao, PNO1 promotes the progression of osteosarcoma via TGF-β and YAP/TAZ pathway. Sci. Rep. 2023;13(1):21827. Published 2023 Dec 9. doi:10.1038/s41598-023-49295-8.
[35] Q. Wang, D. Liang, P. Shen, Y. Yu, Y. Yan, W. You, Hsa_circ_0092276 promotes doxorubicin resistance in breast cancer cells by regulating autophagy via miR-348/ATG7 axis, Transl. Oncol. 14 (8) (2021) 101045, https://doi.org/10.1016/j.tranon.2021.101045.
[36] Y. Chen, H. Yan, L. Yan, et al., Hypoxia-induced ALDH3A1 promotes the proliferation of non-small-cell lung cancer by regulating energy metabolism reprogramming. Cell Death Dis. 2023;14(9):617. Published 2023 Sep 20. doi:10.1038/s41419-023-06142-y.
[37] J. Ning, Y. Ye, D. Bu, et al., Imbalance of TGF-β1/BMP-7 pathways induced by M2-polarized macrophages promotes hepatocellular carcinoma aggressiveness, Mol. Ther. 29 (6) (2021) 2067–2087, https://doi.org/10.1016/j.ymthe.2021.02.016.
[38] Y. Feng, Q. An, Z. Zhao, et al., Beta-elemene: A phytochemical with promise as a drug candidate for tumor therapy and adjuvant tumor therapy, Biomed. Pharmacother. 172 (2024) 116266, https://doi.org/10.1016/j.biopha.2024.116266.
[39] Z. Jiang, J.A. Jacob, D.S. Loganathachetti, P. Nainangu, B. Chen, β-elemene: mechanistic studies on cancer cell interaction and its chemosensitization effect, Front. Pharmacol. 8 (2017) 105, https://doi.org/10.3389/fphar.2017.00105. Published 2017 Mar 9.
[40] M. Xu, H. Zhou, P. Hu, et al., Identification and validation of immune and oxidative stress-related diagnostic markers for diabetic nephropathy by WGCNA and machine learning, Front. Immunol. 14 (2023) 1084531, https://doi.org/10.3389/fimmu.2023.1084531. Published 2023 Feb 22.
[41] S. Revathidevi, A.K. Munirajan, Akt in cancer: mediator and more, Semin. Cancer Biol. 59 (2019) 80–91, https://doi.org/10.1016/j.semcancer.2019.06.002.
[42] N. Hay, Interplay between FOXO, TOR, and Akt, BBA 1813 (11) (2011) 1965–1970, https://doi.org/10.1016/j.bbamcr.2011.03.013.
[43] B.M. Burgering, G.J. Kops, Cell cycle and death control: long live forkheads, Trends Biochem. Sci 27 (7) (2002) 352–360, https://doi.org/10.1016/s0968-0004(02)02113-8.
[44] T. Zhu, J. Han, L. Yang, et al., Immune microenvironment in osteosarcoma: components, therapeutic strategies and clinical applications. Front. Immunol. 2022;13:907550. Published 2022 Jun 1. doi:10.3389/fimmu.2022.907550.
[45] R. Rui, L. Zhou, S. He, Cancer immunotherapies: advances and bottlenecks. Front. Immunol. 2023;14:1212476. Published 2023 Aug 24. doi:10.3389/fimmu.2023.1212476.
[46] M. Li, Y. Yang, L. Xiong, P. Jiang, J. Wang, C. Li, Metabolism, metabolites, and macrophages in cancer. J. Hematol. Oncol. 2023;16(1):80. Published 2023 Jul 25. doi:10.1186/s13045-023-01478-6.
[47] E. Vergadi, E. Ieronymaki, K. Lyroni, K. Vaporidi, C. Tsatsanis, Akt signaling pathway in macrophage activation and M1/M2 polarization, J. Immunol. 198 (3) (2017) 1006–1014, https://doi.org/10.4049/jimmunol.1601515.
[48] A.J. Levine, p53, the cellular gatekeeper for growth and division, Cell 88 (3) (1997) 323–331, https://doi.org/10.1016/s0092-8674(00)81871-1.
[49] K. Tsugawa, M.K. Jones, K. Sugimachi, I.J. Sarfeh, A.S. Tarnawski, Biological role of phosphatase PTEN in cancer and tissue injury healing, Front Biosci 7 (2002) e245–e251, https://doi.org/10.2741/tsugawa. Published 2002 May 1.
[50] A. Nakanishi, Y. Kitagishi, Y. Ogura, S. Matsuda, The tumor suppressor PTEN interacts with p53 in hereditary cancer (review), Int. J. Oncol. 44 (6) (2014) 1813–1819, https://doi.org/10.3892/ijo.2014.2377.
[51] R. Pérez, C. Figueredo, V. Burgos, et al., Natural Compounds purified from the leaves of aristotelia chilensis: makomakinol, a new alkaloid and the effect of aristoteline and hobartine on Na^v channels. Int. J. Mol. Sci. 2023;24(21):15504. Published 2023 Oct 24. doi:10.3390/ijms242115504.
[52] G. Lahmadi, A. Lahmar, M. Znati, et al., Chemical composition and cytotoxic activity of eucalyptus torquata luehm. and eucalyptus salmonophloia F. Muell. trunk bark essential oils against human SW620 and MDA-MB-231 cancer cell lines, Chem. Biodivers. 18 (11) (2021) e2100315, https://doi.org/10.1002/cbdv.202100315.
[53] Q. Fang, T. Que, B. Liu, et al., β-ionone inhibits epithelial-mesenchymal transition (EMT) in prostate cancer cells by negatively regulating the Wnt/β-catenin pathway, Front. Biosci. (Landmark Ed). 27 (12) (2022) 335, https://doi.org/10.31083/j.fbl2712335.
[54] H.EH. Carotenoids, β-apocarotenoids, and retinoids: the long and the short of it, Nutrients 14 (7) (2022) 1411, https://doi.org/10.3390/nu14071411. Published 2022 Mar 28.
[55] L. Sandhiya, H. Zipse, Conformation-dependent antioxidant properties of β-carotene. Org. Biomol. Chem. 2021;20(1):152-162. Published 2021 Dec 22. doi:10.1039/d1ob01723c.
[56] S. Majumder, L. Ren, S. Pushpakumar, U. Sen, Hydrogen sulphide mitigates homocysteine-induced apoptosis and matrix remodelling in mesangial cells through Akt/FOXO1 signalling cascade, Cell. Signal. 61 (2019) 66–77, https://doi.org/10.1016/j.cellsig.2019.05.003.
[57] K. Xu, N. Yin, M. Peng, et al., Glycolysis fuels phosphoinositide 3-kinase signaling to bolster T cell immunity, Science 371 (6527) (2021) 405–410, https://doi.org/10.1126/science.abb2683.
[58] H. Kumagai, A.R. Coelho, J. Wan, et al., MOTS-c reduces myostatin and muscle atrophy signaling, Am. J. Phys. Endocrinol. Metab. 320 (4) (2021) E680–E690, https://doi.org/10.1152/ajpendo.00275.2020.
[59] S. Wang, F. Li, T. Ye, et al., Macrophage-tumor chimeric exosomes accumulate in lymph node and tumor to activate the immune response and the tumor microenvironment, Sci. Transl. Med. 13 (615) (2021) eabb6981, https://doi.org/10.1126/scitranslmed.abb6981.
[60] S.M.P. Vadevoo, G.R. Gunassekaran, C. Lee, et al., The macrophage odorant receptor Olfr78 mediates the lactate-induced M2 phenotype of tumor-associated macrophages, PNAS 118 (37) (2021) e2102434118, https://doi.org/10.1073/pnas.2102434118.
[61] Y. Tao, L. Li, X. Yang, et al., Magnetic-driven hydrogel microrobots for promoting osteosarcoma chemo-therapy with synthetic lethality strategy, Front. Chem. 12 (2024) 1386076, https://doi.org/10.3389/fchem.2024.1386076. Published 2024 Apr 4.